DEFORMATION OF HIGH STRENGTH ALLOYS

AT HIGH STRAIN RATES

By

Sahar Mirfakhraei

A Thesis submitted to the Faculty of Graduate Studies of The University of Manitoba in partial fulfillment of the requirement for the degree of

MASTERS OF SCIENCE

Department of Mechanical and Manufacturing Engineering
University of Manitoba
Winnipeg, Manitoba

THE UNIVERSITY OF MANITOBA

FACULTY OF GRADUATE STUDIES

*****

COPYRIGHT PERMISSION

DEFORMATION OF HIGH STRENGTH ALLOYS AT HIGH STRAIN RATES

BY

Sahar Mirfakhraei

A Thesis/Practicum submitted to the Faculty of Graduate Studies of The University of Manitoba in partial fulfillment of the requirement of the degree

MASTER OF SCIENCE

DEDICATION

To my mother, my father, and my sister whose support and motivation have made it possible for me to finish this project.

ABSTRACT

In this study, the plastic deformation behavior of RHA (Rolled Homogenous Alloy) steel, Aluminum 5083 and Tungsten A 90S were investigated at high strain rates. These three metallic materials are used in armor plate and military applications. The aim of this work is to evaluate dynamic response of the selected armor materials used by Department of National Defense (DND) to mechanical loading at high strain rates and to evaluate the modes of failure in these materials.

The investigated materials were subjected to plastic deformation in compression at high strain rates using direct impact Hopkinson Pressure Bar (HPB). This testing procedure involves striking cylindrical specimens of the materials with a projectile at high impact momentum. The firing pressure of the projectile was varied to produce different impact momentums. The strain rate produced in the test materials on impact is a function of the impact momentum. Dynamic stress strain curves showing deformation stages were generated. The impacted samples were subjected to microscopic evaluation to determine microstructural evolution in the materials during deformation. The objective is to determine failure and deformation mechanisms under extreme loading conditions as in the case of ballistic impact. These investigations show that thermo-mechanical instabilities leading to strain localization and occurrence of Adiabatic Shear Bands (ASBs) dominate the deformation and failure mechanism of these materials at high strain rates and high strain. ASBs are regions of extreme strain localization and are usually harder than the bulk material. They provide preferred crack initiation sites at high strain rates.

The influence of strain rate and impact momentum on shear strain localization was in the materials of interest were investigated. The test specimen samples were tested at different firing pressure ranging from 180-400 kPa for steel samples, 80-200 kPa for aluminum alloy and 200-340 kPa for tungsten samples. This range of firing pressure of the gun produces impact momentum that varies between 40 kg.m/s and 60 kg.m/s for the hardened steel projectile weighing about 1.905 kg.

Microscopic evaluation of the test samples that were cut from RHA steel after high velocity impact shows formation of both white etching bands and deformed bands depending on the impact momentum. At impact momentum lower than 44.53 kg.m/s, no shear band was observed. Deformed bands were observed in samples impacted at 46.6 kg.m/s while formation of white etching bands occurred in samples impacted at samples impacted at momentums above 47 kg.m/s.. The hardness in the shear bands region is much higher that in the bulk material. It was also found that the width and the hardness of the white etching bands that are formed in the steel specimens are influenced by the applied impact momentum. The width of the shear bands becomes wider and the hardness of the shear bands increases as the impact momentum increases.

Deformed bands were observed in both tungsten and aluminum alloys. As the impact momentum increases for RHA Steel and tungsten alloy, the ultimate stress increases until it reaches the impact momentum that causes the formation of adiabatic shear bands. The flow stress then decreases with further increase in impact momentum. In aluminum alloy, as the impact momentum increases, there is no significant changes in maximum flow stress, and the plastic deformation is dominated by adiabatic heating and occurrence of shear band.

ACKNOWLEDGMENTS

Appreciation is expressed to those who have reviewed or made contribution to this project. I would like to thank every one who helped me during this study and guide me to complete this work.

My appreciation goes to my parents, my sister and my very good friends for their patient and support. I am very grateful to my advisor, Professor M.N. Bassim, for all his encouragements and guidance. I would like to thank Dr. Odeshi for all his help and support through this work. I couldn't have done this work without his endless support.

My gratitude also goes to Dr Ojo for his time as my committee member. To Dr Polyzois, my external examiner; I say thank you for your time. I would also like to thank Dr Kuhn, head of the department, for attending my defense. My thanks also go to my very dear friend, Amir, for all his help in the past few months with the revision of the thesis.

I would like to thanks Madame Monon Bolduc and Department of National Defense, DRDV Valcartier for sponsoring the research and paying the research assistantship and supplying the material for my study.

I would also like to thank the department technicians, office support staff and every one who contributed to this work.

TABLE OF CONTENTS

TABLE OF FIGURES

LIST OF TABLES

1 CHAPTER ONE: INTRODUCTION

When a material is deformed under quasi-static loading or at low strain rates, the heat that is generated during the deformation process is conducted away from the sample without even affecting the properties of the material. But at high strain rate the energy dissipation into heat would cause a temperature rise in a localized area of the material, leading to adiabatic heating and subsequently to shear strain localization along narrow bands called ASBs and shear failure. It is adiabatic since there is not enough time for the heat to be conducted out of the hot and severely deformed region.

ASBs are formed when the strain hardening effect of plastic deformation is overshadowed by the thermal softening effect due to local rise in temperature. ASBs are generally harder and more brittle than the bulk material and are usually the cause of failure during dynamic loading at high strain rates. Many failures under dynamic loading have been traced to formation of adiabatic shear bands, which subsequently crack and lead to material fragmentation. There are two types of ASBs in the literature: deformed bands and transformed bands that are also called white etching bands. Deformed bands are similar to the bulk material but they consist of highly distorted grains. Transformed bands appear as distinct white bands when observed under optical microscope. The reason they are called transformed bands is because the white bands are considered to be the product of phase transformation to untempered martensite on rapid quenching by the surrounding matrix [19]. ASBs act as a crack initiation site during high strain-rate loading leading to unexpected failure.

Factors such as thermal softening, geometry of the specimens, strain rate exponent, strain arte sensitivity , presence of cavities, material hardness, microstructure, presence of imperfections, and heat treatment affect the formation of adiabatic shear bands. The early investigations of ASBs were mostly focused on their initiation and propagation from the perspective of both material science and solid mechanics. A recent investigation by Al-ameeri [1] shows the effect of high-temperature treatment on the structure of the white etching bands. Her investigation proves that heat treatment procedure could remove adiabatic shear bands.

The present investigation is carried out to evaluate dynamic response of selected armor materials used by Department of National Defense (DND) to mechanical loading at high strain rates. These metallic materials that were chosen by DND include RHA steel plate, aluminum 5083 H131 and tungsten A90S. These materials are used as armor plates in military vehicles. Although mechanical data for these materials under quasi-static loading are available in the literature. Generation of mechanical data that can be used for simulations and modeling of their response to mechanical loading at high strain rates is becoming increasingly very important for a better material and mechanical design that can provide adequate protection for armed services personnel. The objective of this work therefore is to obtain relevant mechanical properties for these materials under extreme conditions of high strain rate similar to those obtained in the military and defense applications. Further investigation is aimed at analyzing factors such as strain rate on the formation of ASBs and the modes of failure in these three metallic materials.

2 CHAPTERT TWO: BACKGROUND AND LITERATURE REVIEW

2.1 Elastic and plastic behavior of materials

Elastic strain or elastic deformation is a transitory dimensional change that exists only while the initial stress is applied and immediately disappears upon removal of the stress. The applied stress causes the atoms to move from their equilibrium position, while maintaining their relative geometry. When the stress is completely removed, atoms return to their original position and no permanent deformation occurs. Elastic deformation involves stretching rather that breaking the bonds between atoms. Consequently, when the applied load is removed, the material reverts to its original, undeformed condition.

Unlike elastic deformation, plastic deformation is not recoverable and all the changes are permanent. Plastic strain or plastic deformation is a dimensional change that does not disappear when the initial stress is removed. Plastic deformation involves breaking the bonds and making new bonds and is therefore permanent. Ductile materials unlike brittle materials undergo elastic deformation followed by large plastic deformation.

2.1.1 Ductile Material

Ductile materials such as steel and aluminum initially undergo elastic deformation followed by large plastic deformation when subjected to mechanical loading. Three main areas can be recognized in the stress-strain curves for ductile materials: The elastic zone, strain hardening, and necking and rupture. Ductile materials also exhibit distinct ultimate and fracture stresses. The ultimate stress is the highest point on the stress-strain curve and

the fracture stress is the stress at which the specimen fails. During necking, the cross-sectional area starts to decrease in the necking region and that result in formation of many micro-voids and these micro-voids eventually form a crack. Formation of the crack would cause the effective cross-sectional area of the specimen to decrease excessively so that the specimen fails (Fig2.1).

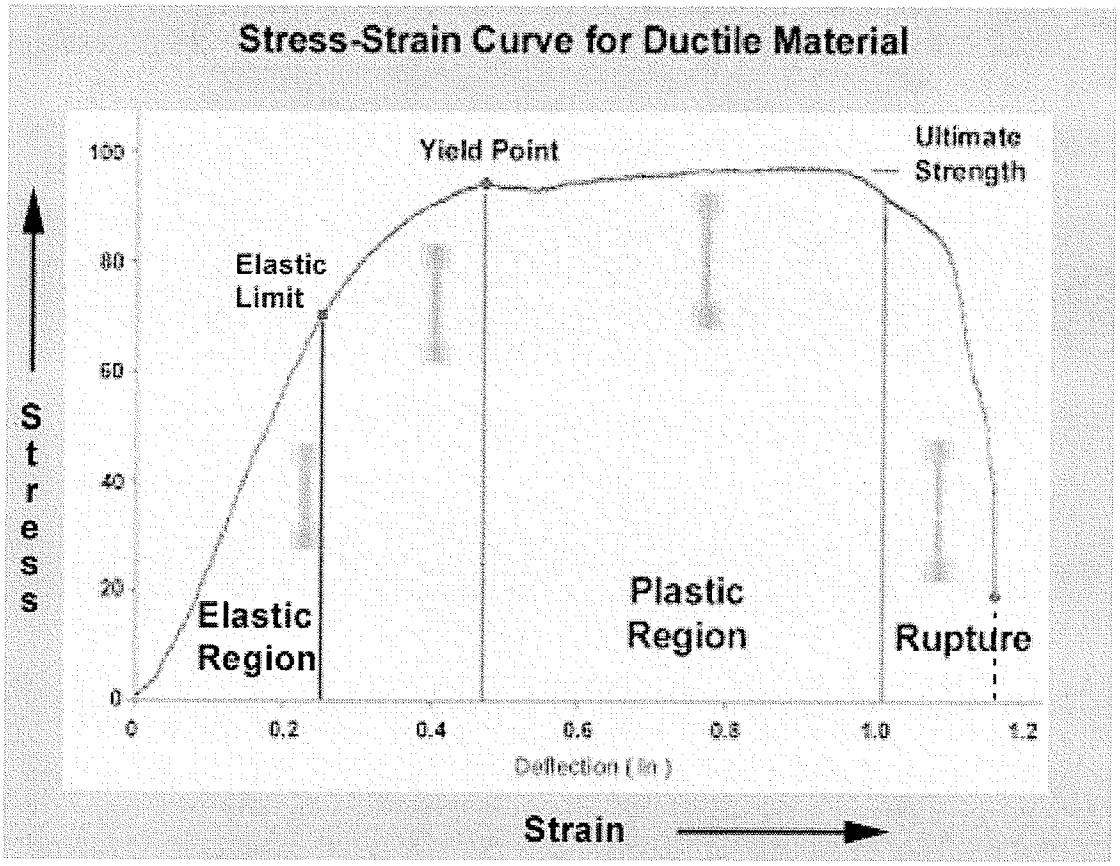

Fig 2.1: stress –strain curve for a ductile material [2]

2.1.2 Brittle Material

A brittle material behaves differently from ductile materials during mechanical loading.

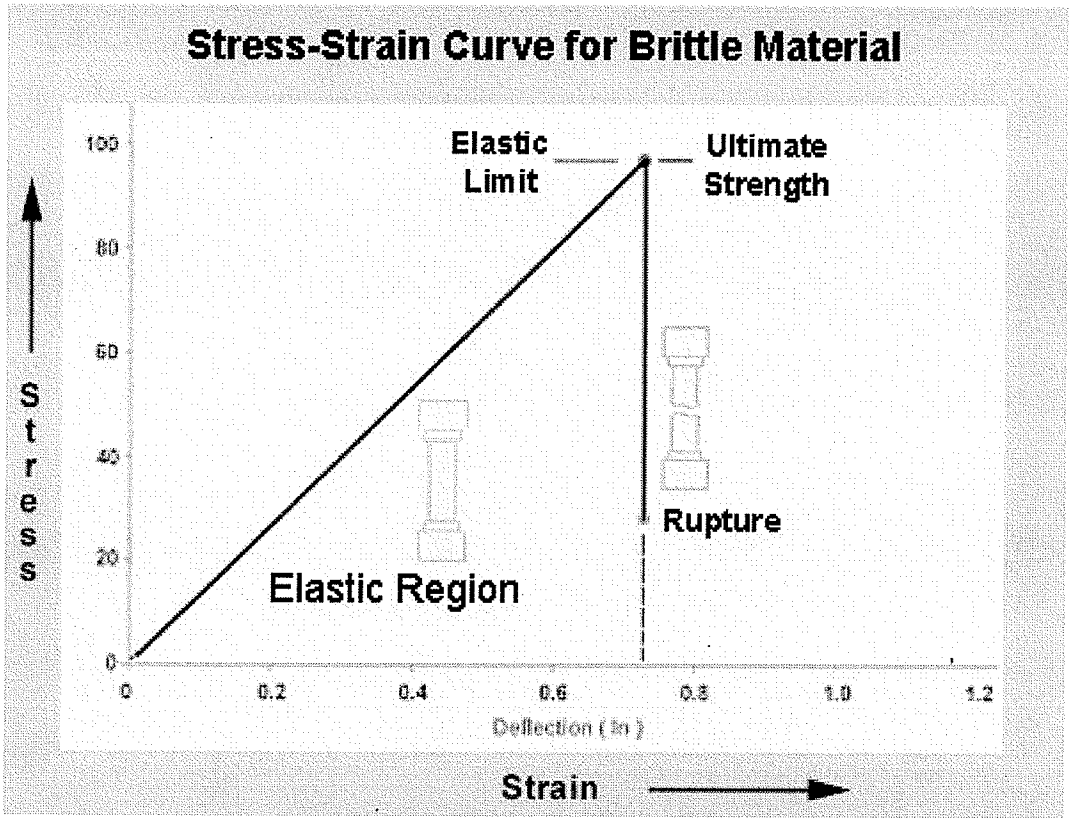

Fig 2.2 stresses –strain curve for a brittle material [2]

The most distinctive difference between the ductile material and a brittle material is that the fracture stress and the yield stress for a brittle material are about the same unlike what is obtainable in ductile materials. The brittle material has an unpredictable failure in that they show a little or no plastic deformation before failure and their strain is usually lower (Fig2.2).

Material behavior also changes with temperature. For example, at very low temperatures (below 0 °C) steel exhibits brittle properties, while at high temperatures it shows ductile properties.

2.1.3 High strain rate deformation

Deformation and failure mechanism in materials at high strain rates is different from that at low strain rates as mentioned above. High strain rate deformation has been shown to produce phenomena such as strain hardening, thermal softening, and phase transition that affect the strength of most materials. At the start of plastic deformation strain hardening controls the deformation process, and deformation is homogenous. As deformation proceeds, adiabatic heating can occur in a narrow region and thermal softening dominates the plastic deformation leading to formation of adiabatic shear bands. In this case, the instability results in thin regions of highly deformed material, which are often the sites of further damage and complete failure. By examining the microstructure of the material after deformation at such high strain rates, it is easy to see the extensive plastic deformation of the grains, fragmentation of the grain, and rotation of particles, precipitates, and cracks [3]. By rapidly deforming the material at different loading rates, it becomes easier to predict when failure occurs and which conditions promote adiabatic shearing and the subsequent shear failure. These strain localizations occur in a narrow region called adiabatic shear bands. ASBs are usually more brittle than the bulk material and can act as precursors to failure during dynamic loading. Many cases of failure under dynamic loading have been traced to formation of adiabatic shear bands, which subsequently crack and lead to materials fragmentation.

2.2 Adiabatic shear bands (ASBs)

Adiabatic shear bands (ASBs) are narrow regions of highly localized plastic deformation induced by large local rise in temperature in a material during dynamic mechanical loading at high strain rates [4-6]. Adiabatic heating usually occurs when the heat generated in the microstructure is retained leading to local rise in temperature. This localization of the deformation occurs when the strength loss from the work softening process becomes greater than the strength increase due to work hardening. The thermal softening process allows the metal to continue deforming rather than fracture and is of great importance in the development of shear bands [7]. In this case, the instability results in thin regions of highly deformed material, which are often the sites of further damage and complete failure [6, 8-11, Fig 2.3].

In the process of adiabatic shear band formation, temperature of the localized region rises radically due to the lack of time for the heat, generated by the deformation, to be released to the exterior. Such a radical local temperature rise has a softening effect, accelerating plastic instability as well as inducing micro-structural modifications such as phase transformation and recrystallization [3]. This also reduces the load-carrying capacity within the ASBs, causing final failure of the structure. Thermal softening, strain rate, plastic strain, and friction have an effect on the deformation localization. It is has also been found that the impact speed and the geometry constraints, have a significant effect on shear strain localization [12-14, 15-20]. Factors such as grain rotation, grain size, microstructure, presence of imperfections and heat treatment affect the formation of ASBs and are explained in detail in section 2.4. When the material cools down to ambient temperature the regions where shear bands regions are usually harder than the bulk

material and exhibit a higher cracking tendency leading to unexpected failure in many cases [4-6].

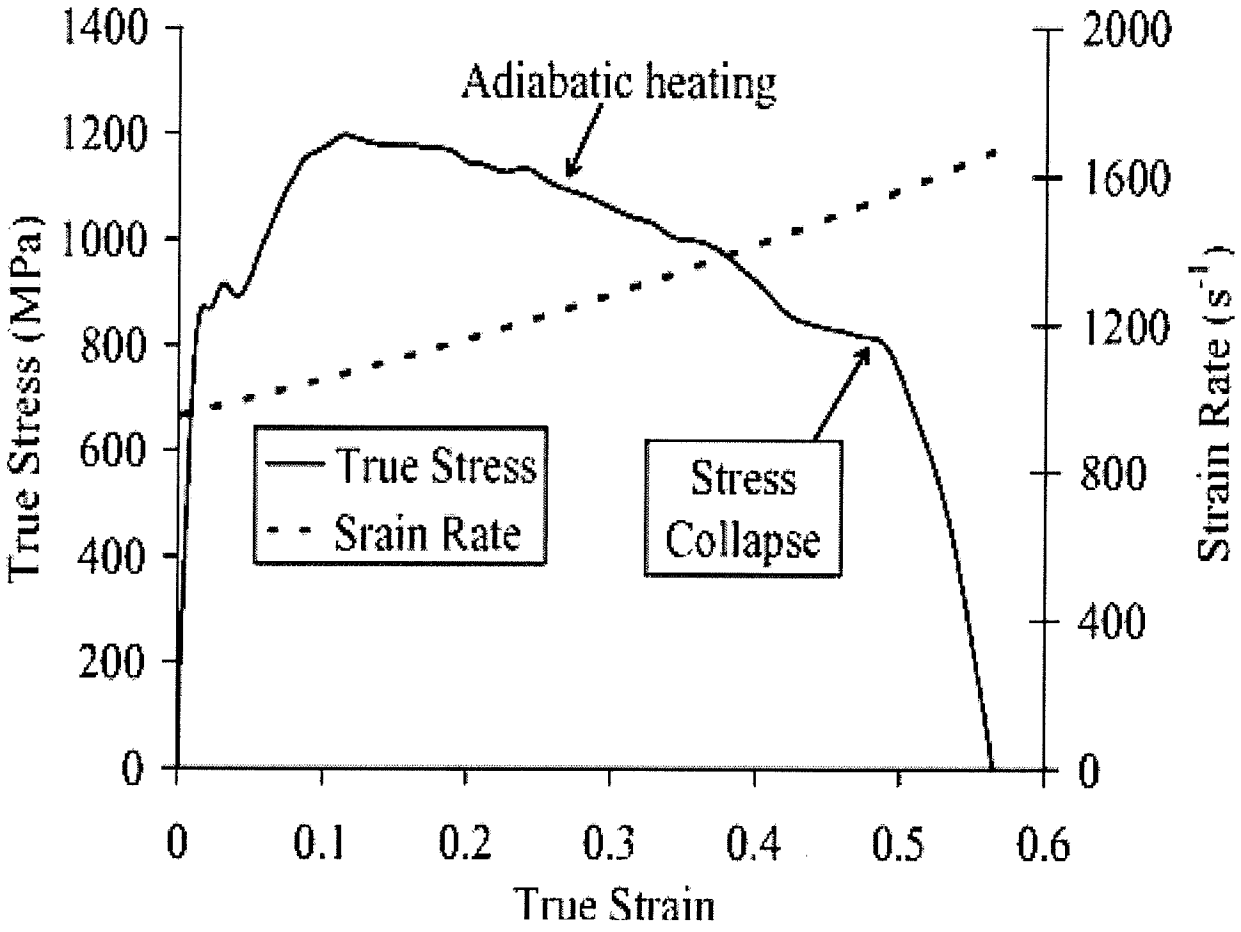

Fig. 2.3: Typical dynamic stress–strain curve for the impacted samples [7]

2.2.1 Microstructure and properties of ASBs

There are two different types of ASBs that are formed in metallic materials at high strain rates, deformed bands and transformed bands (Fig 2.4). Deformed bands are narrow bands showing extensive strain localization, which are similar to the bulk material. The deformed bands are commonly observed in non-ferrous alloys such as copper, tungsten, and aluminum [21]. Transformed bands are also called white etching bands because they appear as distinctive white bands when observed under an optical microscope. The reason that they are called transformed bands is phase transformation that leads to the observed color change which occurs in the shear bands during adiabatic shearing. The white color of the bands is due to their austenization during adiabatic heating and subsequent transformation to martensite [22].

Transformed bands observed in massively and rapidly deformed steels are known to contain very fine sub-grains of a few hundred nanometer size. Transmission Electron Microscopy (TEM) investigation by Derep [23] shows that the microstructure of transformed bands in armour steel consists of very fine martensites, iron carbides and ferrites having dimensions below 300 nm. Cho et al [24] attributed the formation of the very fine cells in transformed bands to elongation and fragmentation of the existing grains along a shear band propagation path during deformation. They observed two microstructures in the center of the shear bands: a) highly elongated narrow sub-grains (laths) that are extended in the shear direction and b) fine equi-axed cell with high dislocation densities. Schematic illustration of the microstructural evolution during adiabatic shearing by Cho and his colleagues is given in Fig 2.5.

Elongation, fragmentation and spheroidization of the cementite layer in pearlitic steel have also be reported inside shear bands by Zurek [15], who measured the size of spheroidized cementite to range from 0.01 and 0.05 μm. Zurek attributed the white color of a transformed band to the resolution limit of an optical microscope in resolving the nanoscaled structure of the shear band. Meyers et al [25] suggested that microstructural evolution at high strain rates begin with a homogeneous distribution of dislocations that rearrange themselves into dislocation cells which eventually become elongated sub-grains that subsequently break down into equi-axed microcrystalline structure as strain increases. The investigation by Meyers et al [25] on microstructural evolution in stainless steels at high stain rates show that evolved shear bands consist of two regions; one region consists of extremely fine grains (0.1-0.2 μm) with well defined grain boundaries and dislocations, and another region having a glassy structure (solid-state amorphitization).

Armstrong et al [26] have also traced initiation and propagation of ASBs to dislocation pile up that is enhanced by inclusion and precipitates. He observed a transition at high strain rates from plasticity being controlled by movement of originally-resident dislocation density to the strain rate being controlled by dislocation generation at the shock front. Armstrong and Zerilli [26] suggested that a local rise in temperature and softening can be produced when a dislocation pile-up pierces through a grain boundary creating a site for shear band initiation. TEM investigations on α-titanium by Chichili et al [27] also reveal the following microstructural evolution across the shear bands (a) planar dislocation and twinning; (b) grouping of dislocation into cells; (c) formation of

elongated sub-grains along shear directions; and (d) development of equiaxed nano-crystalline grains 50 – 500 nm in diameter (Fig 2.6).

It is very clear that dislocation mobility and dislocation pile-up play very prominent roles in the occurrence of ASBs which in turn influences dynamic mechanical failure at high strain rates.

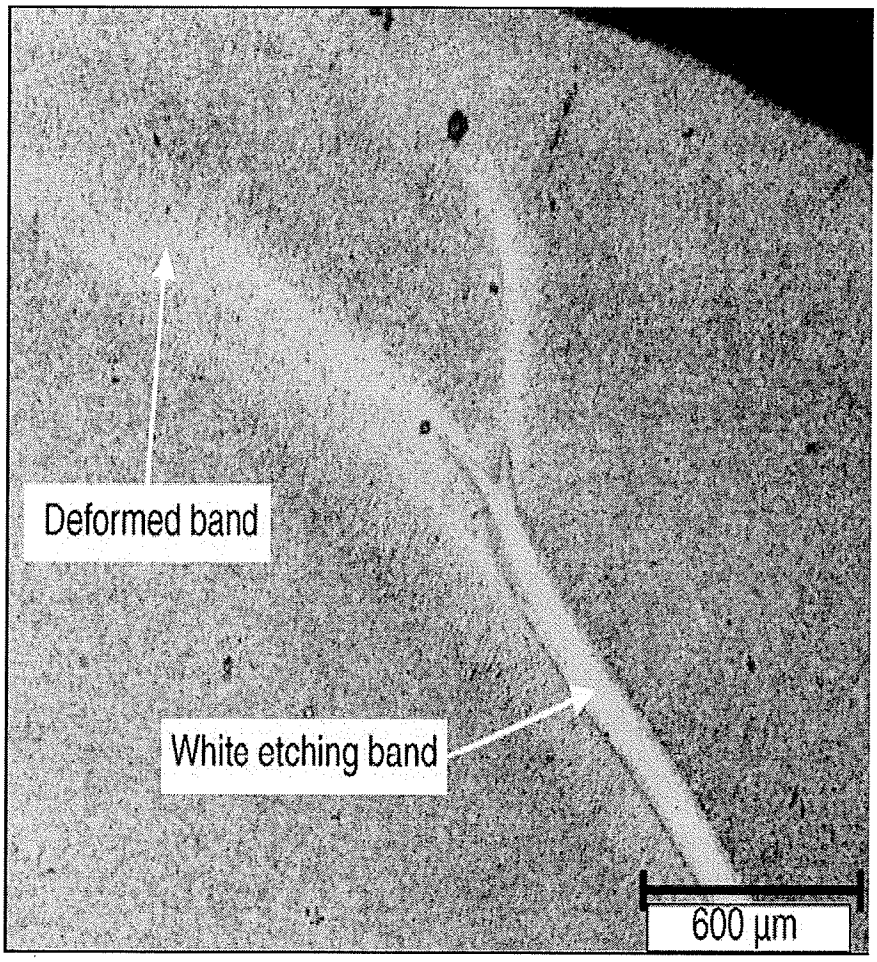

Fig 2.4: Adiabatic shear bands in AISI 4340 steel after a high velocity impact

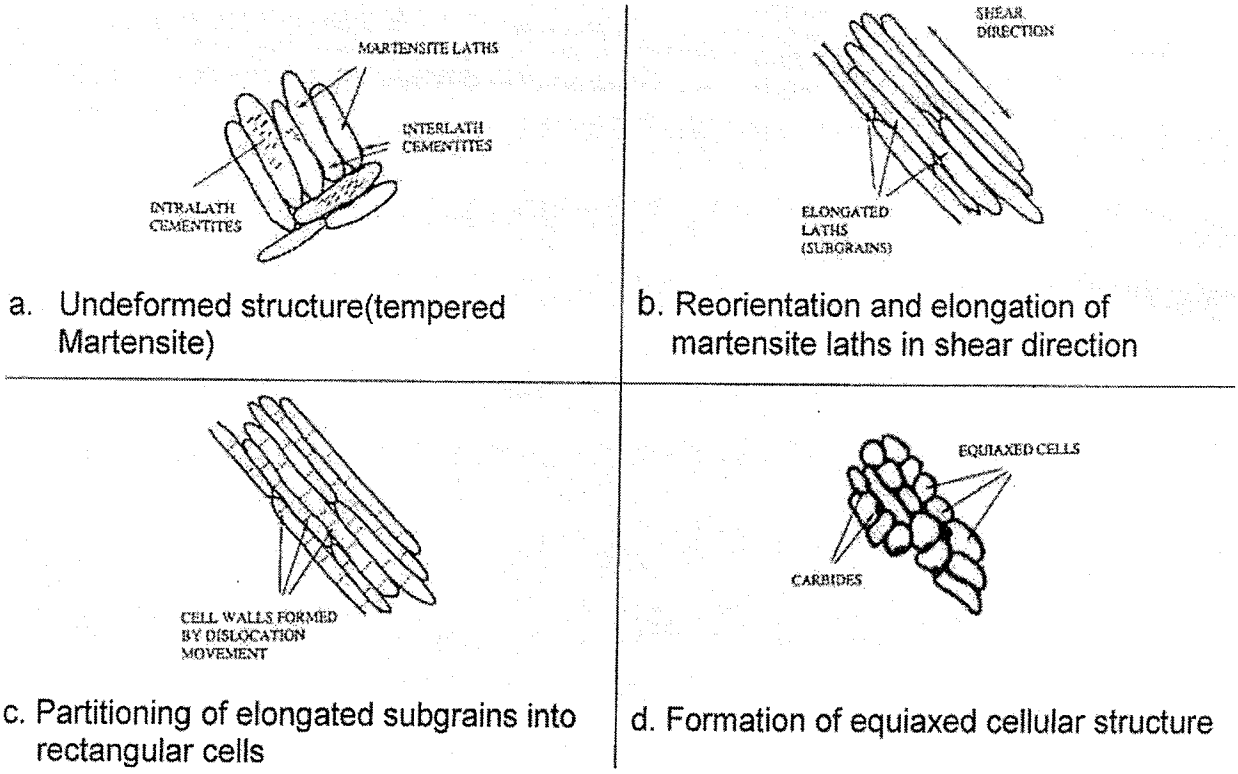

Fig 2.5 Schematic representation of microstructural evolution during adiabatic shearing in HY-100 steel [24]

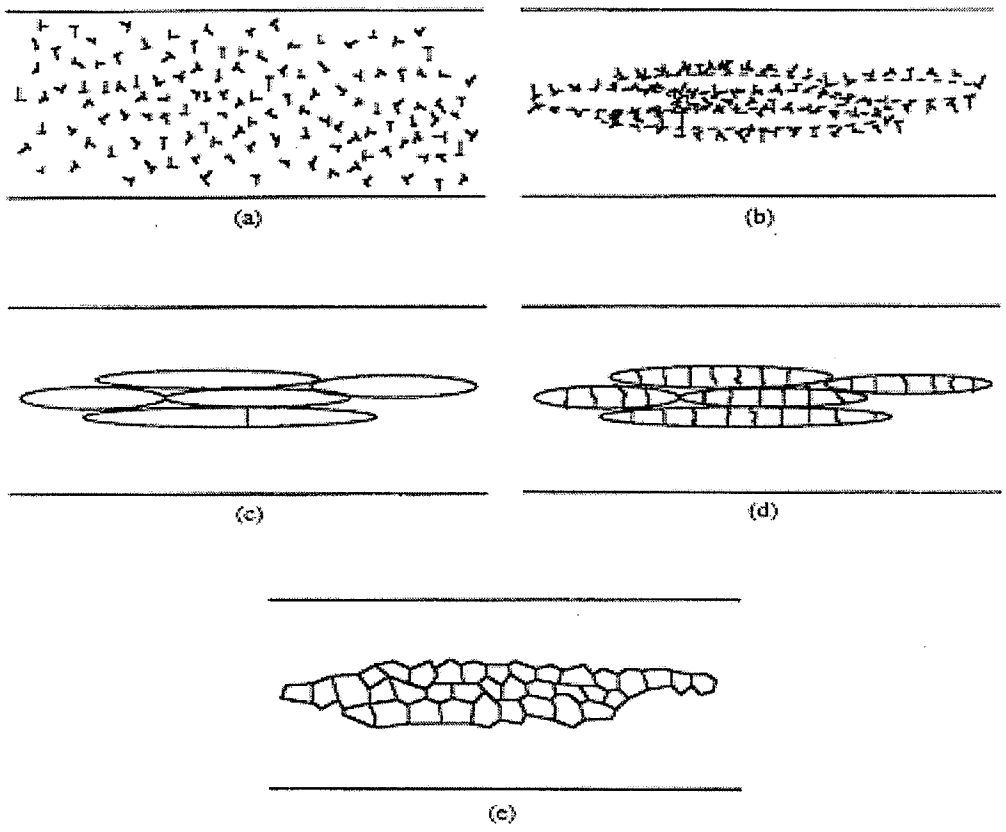

Fig. 2.6: Schematic representation of microstructural evolution in shear bands showing (a) planar dislocation (b) dislocation pile up, (c) elongated dislocation cell formation,(d) break-up of elongated dislocation cell (e) formation of very fine equi-axed grains [27]

2.3 Initiation of Adiabatic shear bands

According to Marchand and Duffy [4], plastic deformation of most metallic materials occurs in three stages which begin with a homogenous strain, followed by a generally inhomogeneous strain. At the last stage of the deformation process, extreme strain localization will occur that results in formation of narrow shear bands (Fig 2.3). Some scientists have different perspective about this process: Wright and Walter [28] have mentioned that the loss in strength of the material has greater influence on the formation of the shear bands than the strain localization. Schoenfeld and Wright [6] have suggested that the stress collapse and adiabatic shear banding occur in the material due to non-uniformity in the microstructure, which may be the result of internal imperfections, porosity, and geometry of the specimen. Feng and Bassim [17] have found that the formation of ASBs can be initiated at local material defects. Li *et al.* [29] have also reported that shear bands were formed initially at the location of maximum shear stress.

Finite element modeling of occurrence of ASBs in high strength low alloy steel by Feng and Bassim [17] have shown that material deformation at high strain rates occurs in three stages. In the first stage there is no plastic deformation. In the second stage, the stain hardening and thermal softening compete with each other. Thermal softening is the result of the conversion of part of the deformation energy into heat energy while strain hardening is due to the increase of the dislocation density during deformation. During the last stage of deformation, thermal softening dominates the deformation process and that leads to the stress collapse, strain localization, and formation of ASBs [9]. Odeshi *et al.* [7] also suggested that at the beginning of the deformation process the flow stress increases with increasing strain and the strain hardening effect of the plastic deformation

controls the deformation process until the maximum flow stress is reached. Beyond the maximum flow stress, thermal softening dominates the deformation process and the flow stress decreases with increasing strain. As strain increases, a critical strain is reached where stress collapse and strain localization along shear bands will occur. The stress collapse occurs due to thermo-mechanical instability caused by excessive heating in the shear band region (Fig 2.3).

2.4 Factors influencing formation of ASBs

Many factors influence formation and propagation of ASBs such as specimen geometry, surface friction, heat capacity, heat conductivity, strength level, thermal softening, chemical composition, strain rate, microstructure, and presence of imperfections. It is also been found that heat treatment has a significant effect on shear localization [13].

It has been reported that the materials with high thermal softening, high value of hardness, but low strain rate sensitivity and low thermal conductivity are more susceptible to formation of ASBs [15, 16].

The grain size has an effect on initiation of shear bands. Larger grains exhibit a lower yield stress and smaller grains have a higher yield stress. The larger grain will deform preferentially and could be an initiation site (30, 31 and Fig 2.7 (a)).

Grain rotation can lead to softening which could be the cause of initiation of shear bands (30,31 and Fig 2.7 (b)) and dislocation pile-up passing through a grain boundary can generate a local rise in temperature and plastic deformation that could initiate strain localization and occurrence of adiabatic shear band [30,31,Fig 2.7(c)].

- **In Steels**

It has been suggested by Zurek [15] that formation of cracks in steel samples under tensile test would prevent sufficient localization of deformation unlike what is observable in compression at high strain rates. He observed that the fracture due to the formation of crack in the impact testing is caused by the localized adiabatic heating and the formation of adiabatic shear bands. Microstructure plays a significant influence on the type of ASBs that is formed in steel at high strain rates. Rogers and Shastry [19] recorded the formation

of white etching bands in quenched and tempered AISI 1018 steel while Meyers and Wittman [20] observed deformed bands in the same steel samples but in the normalized condition.

Feng and Bassim [17] reported that the presence of microstructural imperfections and inclusions such as secondary precipitates promote the occurrence of ASBs in steel.

In a recent investigation, Odeshi *et al.* [14] confirmed that heat treatment has a significant influence on the formation of ASBs in AISI 4340 steel samples. Whereas white etching bands are reportedly formed in the quench-hardened steel samples that are tempered at 300°C and 400°C, deformed bands are observed in the steel samples tempered at the temperature above 500°C. This shows that increasing the tempering temperature would reduce the tendency for the formation of very hard white etching bands that is highly susceptible to cracking (Fig 2.8).

- **In aluminum alloys**

El-Magd and Brodmann [32] reported that the adiabatic heating during the deformation process in aluminum samples reduces the flow stress and promotes instability. Their investigation proved that under dynamic loading conditions, the stain rate sensitivity of the material increases with increasing strain rate. They also suggested the influence of material parameter and deformation conditions on the formation of adiabatic shear bands. They showed that the geometry of the aluminum alloys plays a major role in the formation of adiabatic shear band. Owolabi *et al.* [33] observed that reinforcing the aluminum alloy with alumina particles increases its strength and stiffness. However, the susceptibility of the aluminum alloy to strain localization and adiabatic shear failure increases with particulate reinforcement. In addition, the particulate

reinforcement leads to cracking of the surface of the impact samples depending on the volume fraction of the particulate reinforcement as well as on impact momentum.

- **In tungsten**

Li suggested [34] that the geometry of the test specimen plays a very important role in the occurrence of adiabatic shear band in tungsten. He used numerical simulation to establish that an uneven stress condition in the specimen is the reason for the initiation and propagation of ASBs. Numerical simulation also reveals the sensitivity of ASB initiation to surface friction.

Kim and Lee [35] have also suggested that the important factors involved in the formation of shear bands are the thermal instability, the microstructural factors such as the shape of the tungsten particles and the characteristics of interface between them. Bose and Couque [36] have suggested that tungsten alloys do not shear adiabatically by themselves. The localized microstructural inhomogeneties such as voids and large matrix pools may act as elements that trigger the shear localization events.

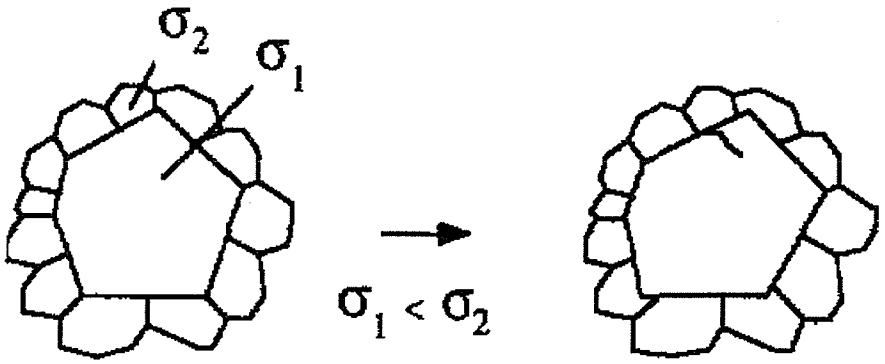

Fig 2.7 (a) Grain size inhomogeneity [31]

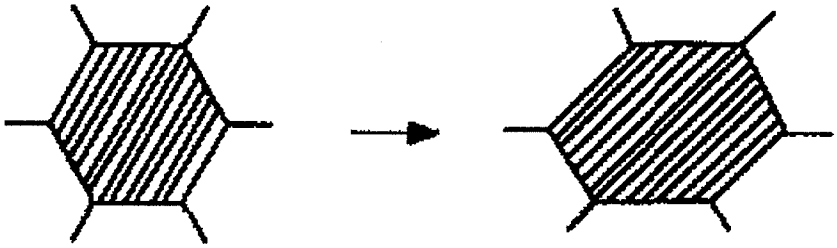

Fig 2.7 (b) Geometrical softening [31]

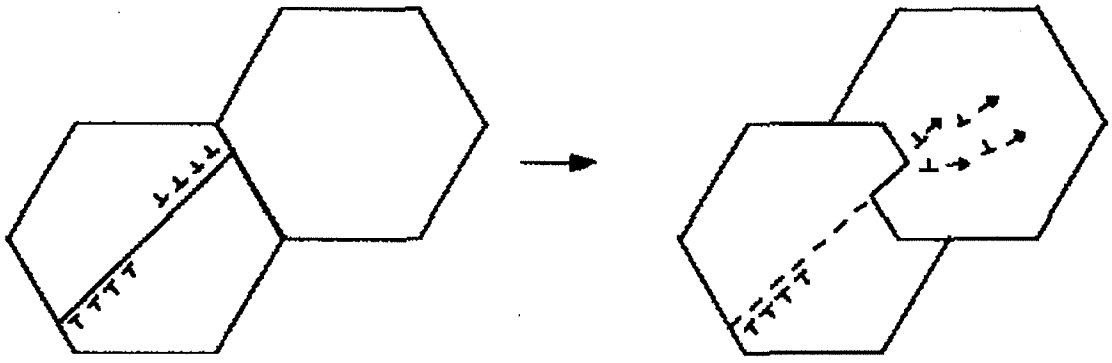

Fig 2.7 (c) Dislocation pile-up releases [31]

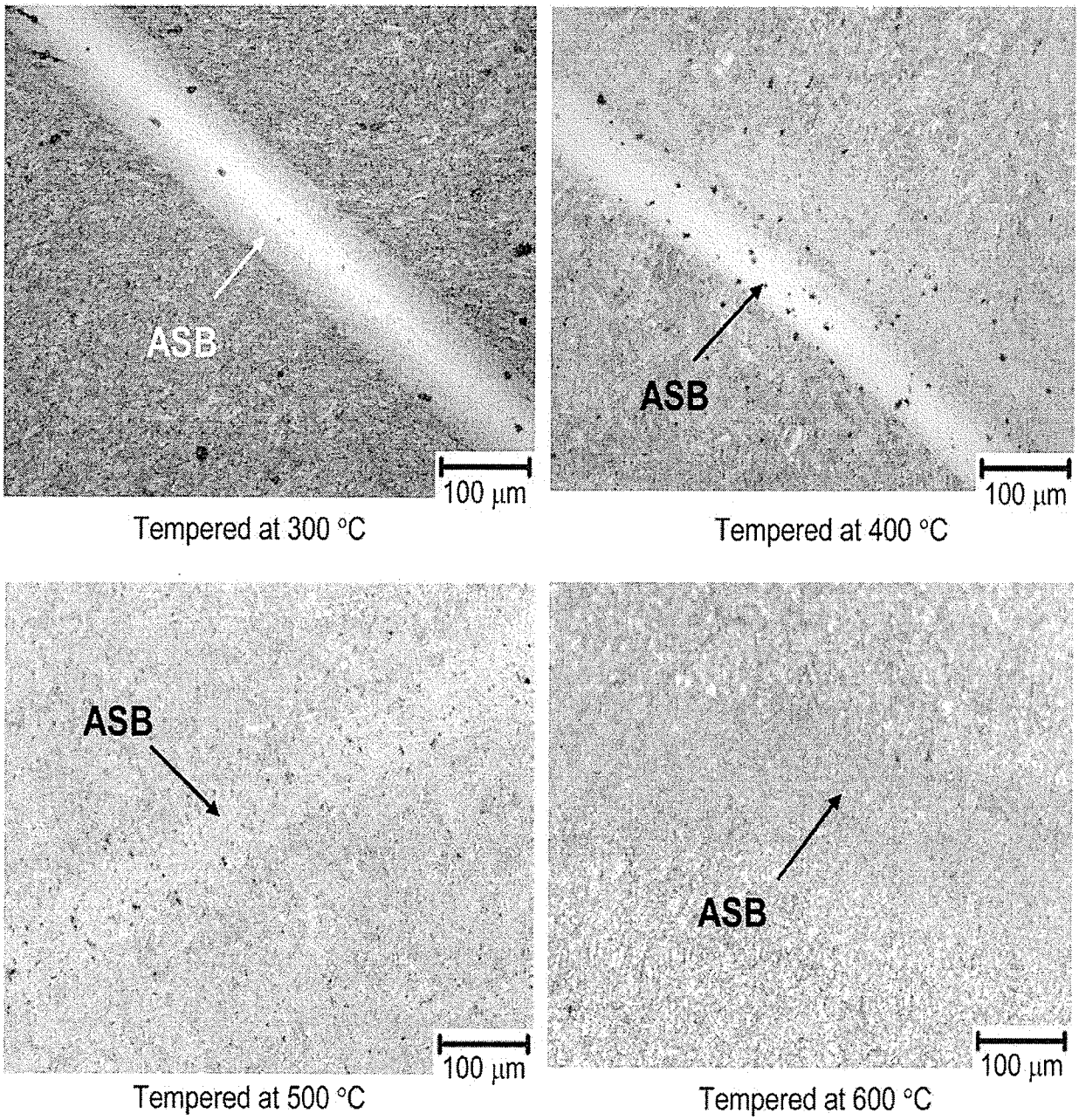

Fig 2.8 Optical micrographs: The effect of tempering temperature on formation of adiabatic shear bands (ASB) in oil-quenched AISI 4340 steel [14]

2.5 Propagation of shear bands and failure of material

As mentioned previously, ASBs initiate at inhomogeneities [12]. Investigations by Odeshi *et al.* [7] showed that fracture of the samples occurs by crack initiation and propagation along the shear bands. The cracks are initiated by nucleation of micro voids which coalesce, grow, and develop into a crack. This investigation also shows that shear bands in the cylindrical steel samples form two conical shells. When they are observed in the transverse section, the bands have circular or parabolic shape depending on the intensity of impact momentum. In between the two circular bands there is an ASB free zone at the middle of the cylinder. If there is a crack initiated on one of the cones, it would propagate through the free zone and continues along the adjacent part until the sample fractures into two parts (Figs 2.9-2.11).

Shear bands have lower flow stress because of the heat that is generated in the material during impact testing. Formation of cracks occurs in three stages. The first stage is the nucleation of voids within the shear bands (Fig 2.12(a)). Most voids are initiated at the width of the band and are elongated to an elliptical shape along direction of the shear band. The second stage is elongation and rotation of voids. Finally at the last stage, voids join together and create cracks [14],(Fig 2.12b). These cracks would propagate and result in failure of the material (Fig 2.12(c)). Feng and Bassim [17] have also suggested that the growth of shear bands is affected by strain hardening, thermal softening, and thermal conductivity.

There are a number of reasons for formation of voids in the material. The high temperatures of the shear band regions make them have lower flow stress than the surrounding matrix and consequently generate tensile stresses that will open up voids in

the shear bands [37, 20, and 38]. In addition to the theory of tensile stress opening up voids in shear bands during thermal softening, cavitations growth by atomic mobility at high temperature has also been proposed for voids nucleation in ASBs [39]. The equilibrium number atomic vacancies (N_V) caused by atomic mobility are known to increase exponentially with absolute temperature (T) as follows:

$$N_v = N \exp\left[\frac{-Q_v}{RT}\right] \qquad (2.1)$$

Where N is the total number of atomic sites, Q_V the activation energy require to produce one mole of vacancies and R the general gas constant. The high temperature in the shear bands during adiabatic shearing will therefore promote formation of vacant lattice sites in the bands.

Shear bands are usually harder and more brittle that the bulk material. Moreover, they have a higher cracking tendency. Increase in hardness makes the material more brittle and more subject to cracking. Dong-kuk and Sunghak Lee [35] suggested that when shear bands are formed, hardness of the central area of the bands increases and resistance to applied load is radically reduced, inducing easier initiation and propagation of cracks in the area and results in failure of the material

Meyers [37] suggested that cracks initiate and propagate within the shear bands and more often they intersect with each other, causing failure. The mechanism of plastic deformation at high strain rates such as ballistic impact is a complex phenomenon that is dominated by strain localization along narrow bands. Most unexpected failure of

materials under impact loading has been traced to this strain localization during deformation.

The objective of this study is to investigate the mechanism of plastic deformation and occurrence of strain localization and adiabatic shear banding in Rolled Homogeneous Armor (RHA) steel, Tungsten heavy alloy (WHA) and aluminum 5083 H131 alloy. The aim of this work is also to evaluate and to compare the dynamic response of these selected armor materials use by the Department of National Defense (DND). These are armored material used in military applications and constantly exposed to high strain-rate deformation in service.

This thesis is mainly focused on the influence of the impact momentum on the deformation mechanism and analysis of the modes of failure in these three metallic materials.

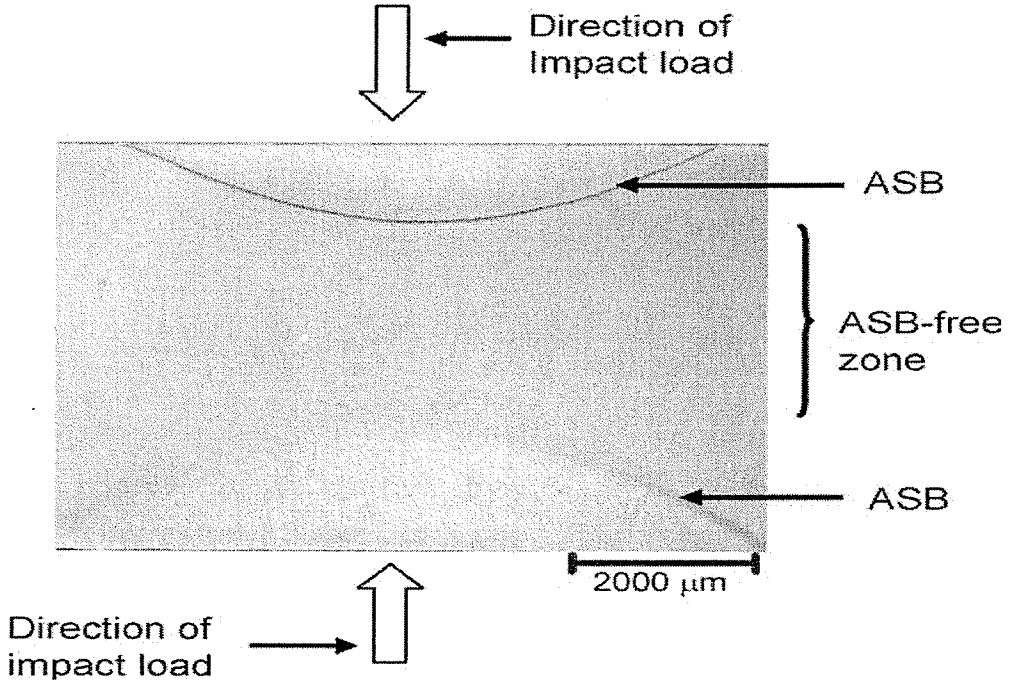

Fig 2.9 Macro-structure of transverse section of a sample after Impact testing [14]

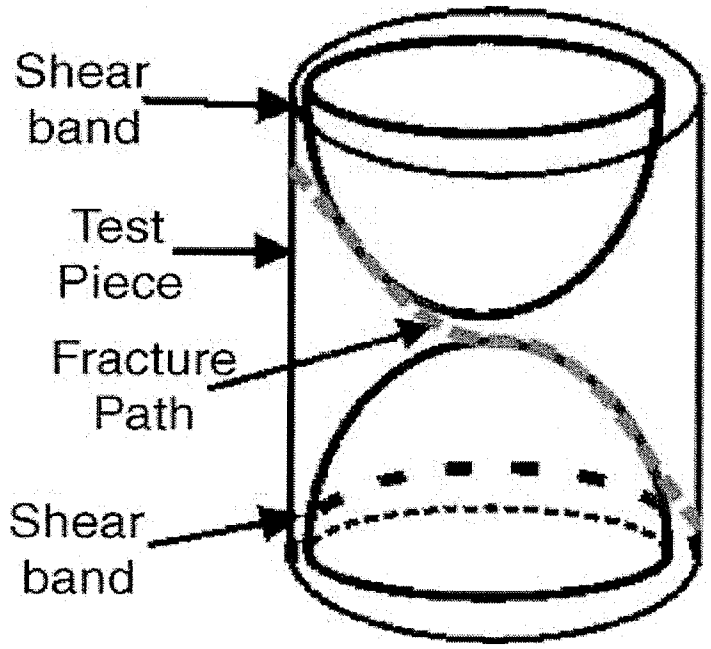

Fig 2.10 Schematic representation of fracture path in failed samples during impact testing [14]

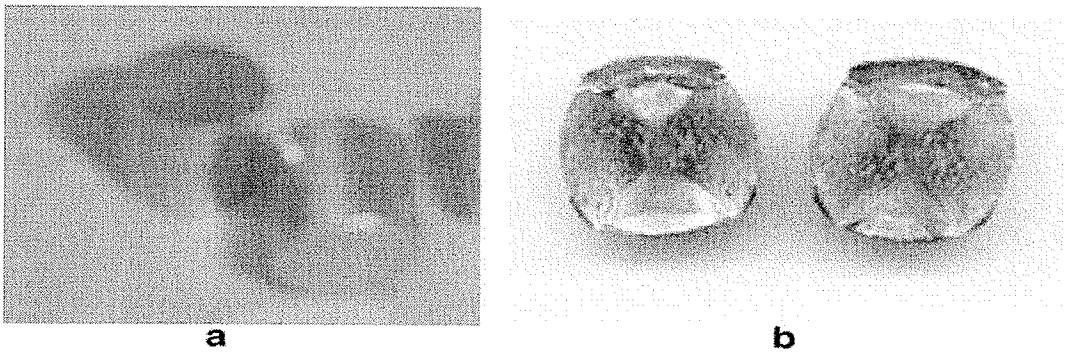

Fig 2.11 Tested samples (a) before impact and (b) after fragmentation under impact loading [14]

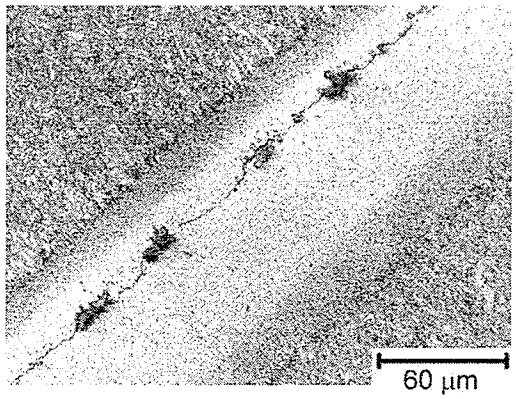

(a)

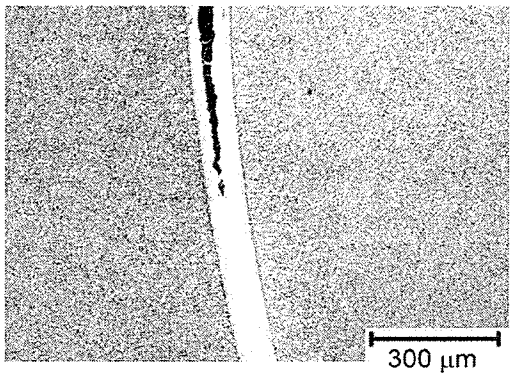

(b)

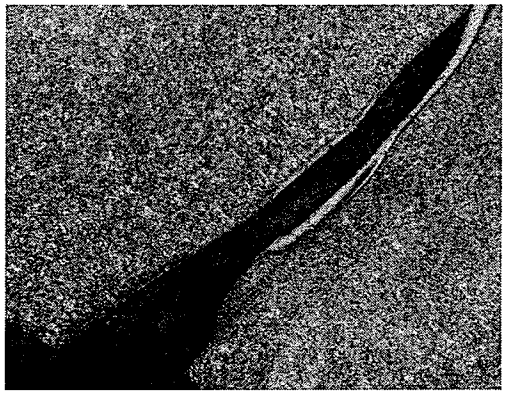

(c)

Fig 2.12 (a) Coalescence of micro-voids generating micro-cracks at the initial stage of cracking , (b) Crack propagation part along a shear band , (c) Failure of the material [14]

3 CHAPTER THREE: EXPERIMENTAL PROCEDURE

3.1 Introduction

This chapter covers:

- Materials used in this study
- Description of the geometry of the specimens
- Use of the Direct Hopkinson Pressure Bar
- Preparation of the specimens for metallurgical analysis
- Micro-hardness measurements.

3.2 Materials

The materials used in this study are:

- Group one: RHA Steel
- Group two: Aluminum 5083 H131
- Group three: Tungsten A 90S

The materials were supplied by DND (Department of National Defense) and were sent to our research group for testing. Test specimens for each material were cut from the same bar as provided by DND.

3.3 Geometry of the specimens

The cylindrical test specimens were 10.5 mm in length and 9.5 mm in diameter. The dimensions were chosen to achieve maximum strain and strain rate in the materials during impact, based on earlier work by Bassim [12].

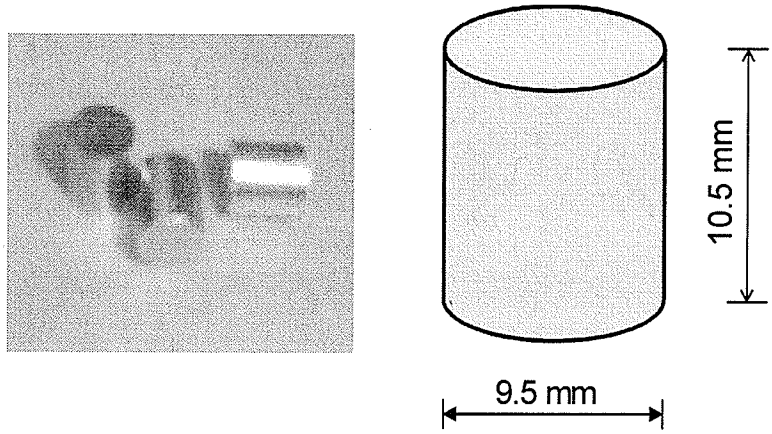

Fig 3.1: Geometry of test specimen for compression test

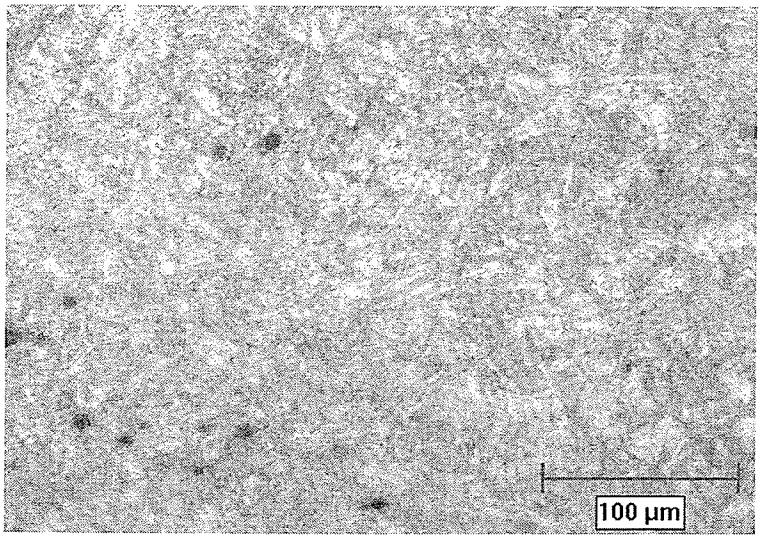

Fig 3.2: Optical micrograph of the investigated RHA Steel in as received condition

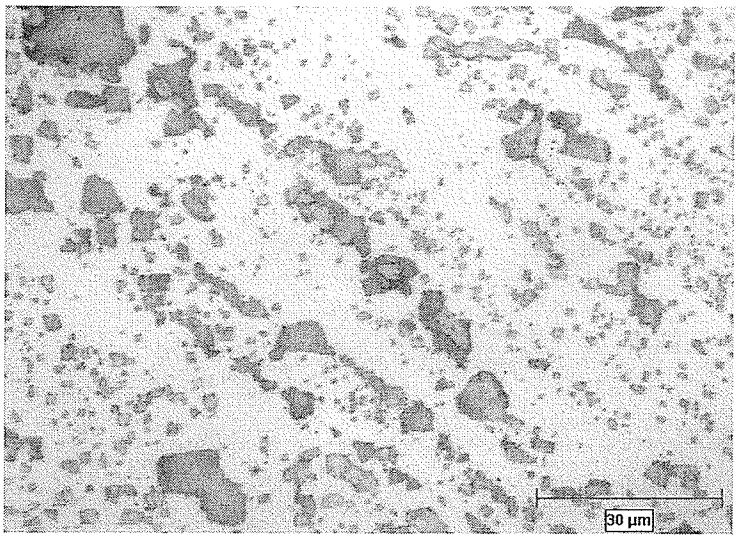

Fig 3.3: Optical micrograph of the Aluminum 5083 in as received condition

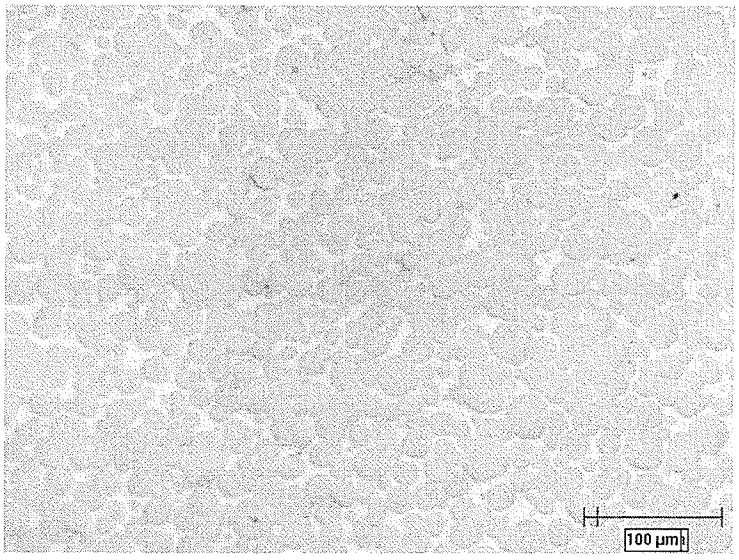

Fig 3.4: Optical micrograph of the Tungsten A90S in as received condition

3.4 Impact Test

The three groups of the investigated materials were impacted using the direct impact Hopkinson Pressure Bar (HPB). The firing pressure for different groups of materials ranged differently. The firing pressure for Steel samples ranged from 140-400 kPa, for Aluminum 80-200 kPa and for Tungsten 200-360 kPa. The firing pressure was varied to investigate the influence of impact momentum on response of the materials to dynamic mechanical loading at high strain rates. The corresponding impact momentums produced by various firing pressures are presented in Table3.1. All impact tests were conducted at room temperature and under atmospheric pressure.

3.4.1 Operation of the Direct –Impact Hopkinson Pressure Bar

The Split Hopkinson Pressure Bar is the most commonly used method for investigating the effect of the high strain rate on different kinds of material. The SHPB, which was developed from Bertram Hopkinson bar by Kolsky in 1949, remains the standard equipment for measuring the response of engineering materials to high strain rate deformation to the range of 10^{3}- 10^{4} S^{-1}. A sketch of the direct impact Hopkinson Bar used in this study is presented in Fig 3.5. The Hopkinson Bar consists of a projectile, pressure vessel, control box, firing barrel, test specimen, strain gage, and transmitted bar, which is 3.8cm in diameter and 1.5m long.

- **Projectile**

The projectile is a cylindrical 4340 Steel bar and it is heat treated to a Rockwell hardness value of 47 HRC with the length of 0.2 m and the weight of 1.905 kg (See Fig 3.9). The projectile is fired using a light gun, which causes a compressive stress wave to travel through the specimen to the transmitted bar.

- **Gun barrel**

A hollow cylinder connected to the gun to guide the projectile toward the sample at high velocity (See Fig 3.8)

- **The Timer**

The time for the projectile to travel and hit the specimens is measured with the use of a timer.

- **Accumulator and firing chamber**

The compressed air in the accumulator is used to produce the pressure in the firing barrel to force the projectile to strike the sample at high velocity. A pressure gage attached to the accumulator measures the firing pressure.

- **Control Box**

The control box is a unit that controls all the various parts of the SHPB and consists of a power switch button, retract/reset button which bring the projectile to the start point, charge button for charging process before firing, accumulator pressure button for controlling the firing pressure, fire button for firing the projectile and a pressure gauge for changing to desire pressure for the impact testing (See Fig 3.6).

- **Transmitted Bar**

The transmitted bar is made of AISI 4340 steel which has been heat-treated to a hardness of 45 HRC. The length of the transmitted bar is chosen in a way that the time for the reflected pulse to arrive at the strain gauge would be greater than the time required for the deformation of the specimen (See Fig 3.7).

The specimen was made to stick to the transmitter bar using Vaseline. The projectile was fully lubricated using Molybdenum disulphide (MoS_2). On firing the gun, the projectile strikes the test samples at a very high velocity (See Fig 3.10). This impact loading of the specimen generates elastic waves which travel through the specimen unto the transmitter bar. The amplified elastic waves are captured by an oscilloscope in the form of voltage- time data. The impact velocity of the projectile is directly proportional to the firing pressure. Some of the tested specimens failed at higher impact velocities. The experimental data sheet is given in Table 3.1. Strain signals were saved by the oscilloscope and transferred to the computer for further analysis.

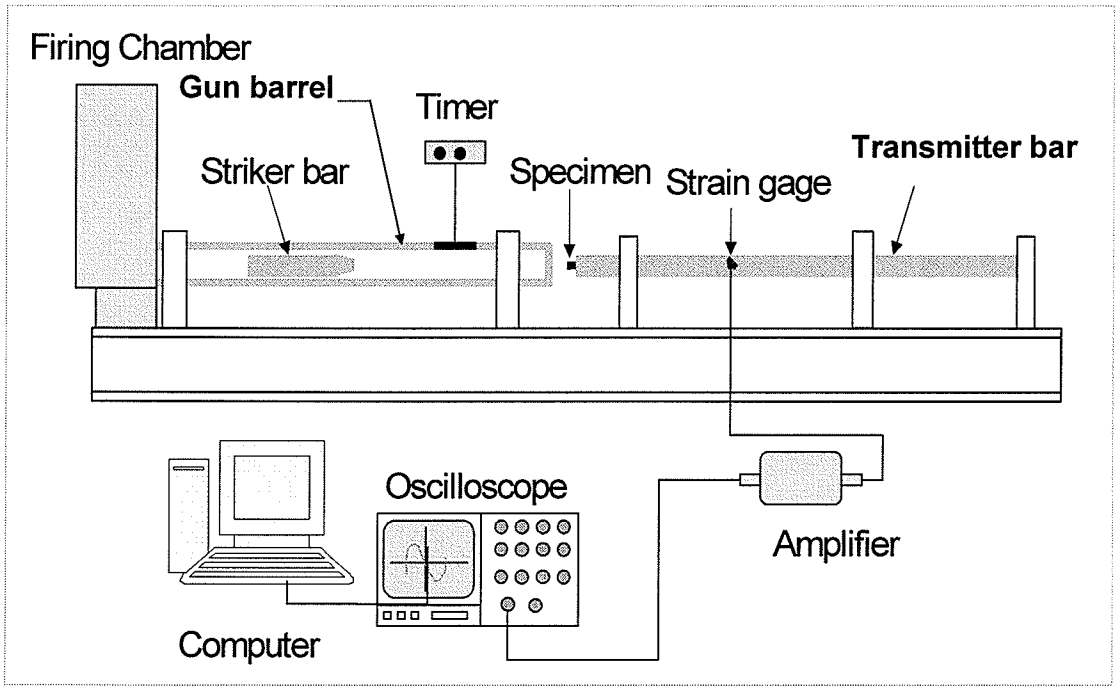

Fig 3.5: Schematic Representation of the Direct Hopkinson Bar

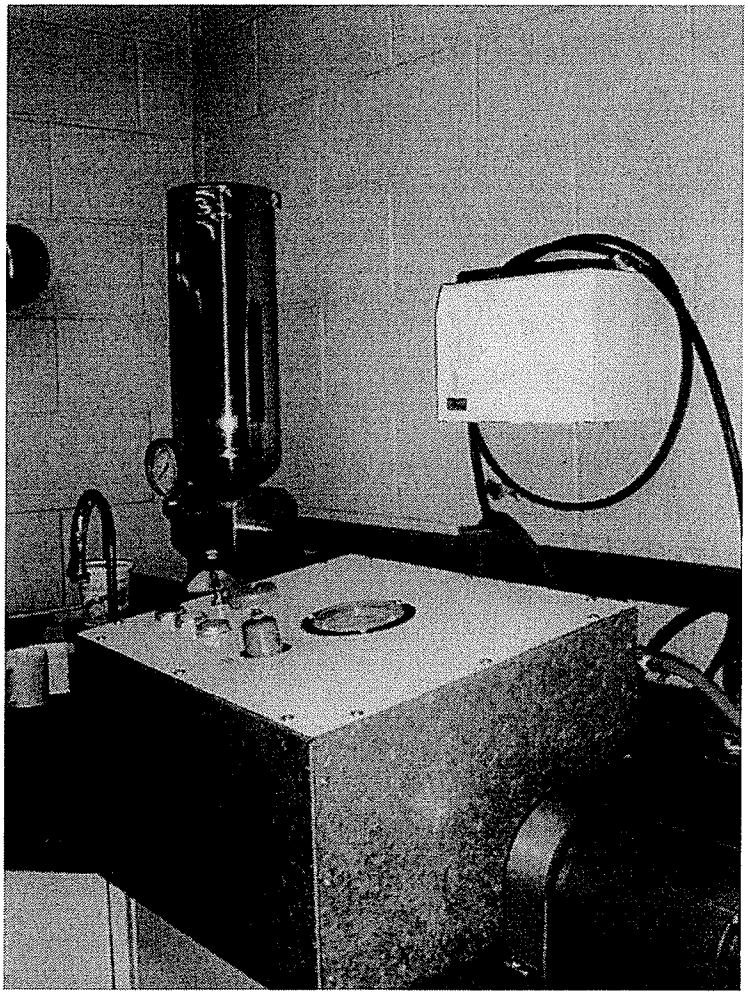

Fig 3.6: Control equipment of SHB

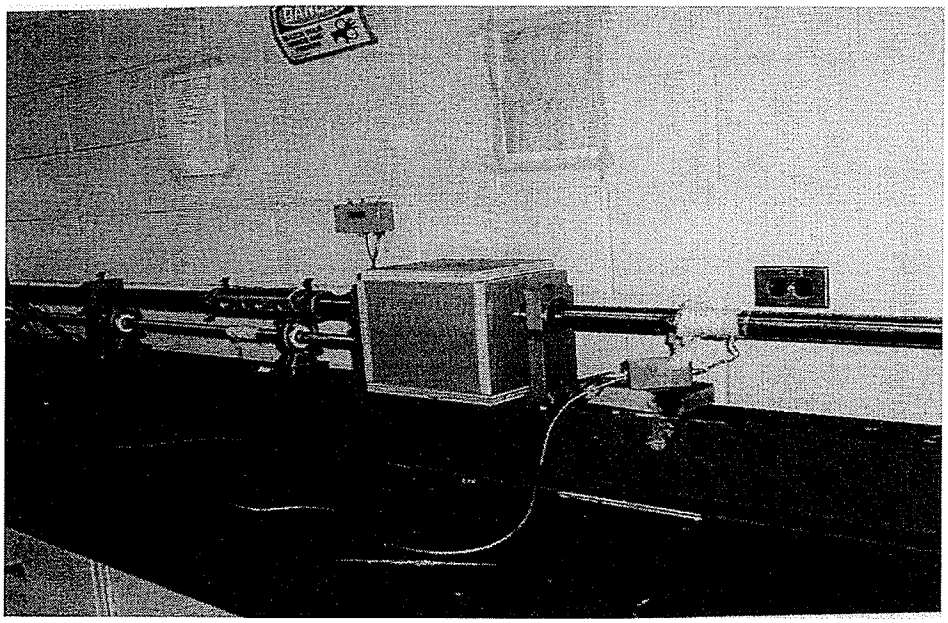

Fig 3.7: Transmitted bar and strain gauge

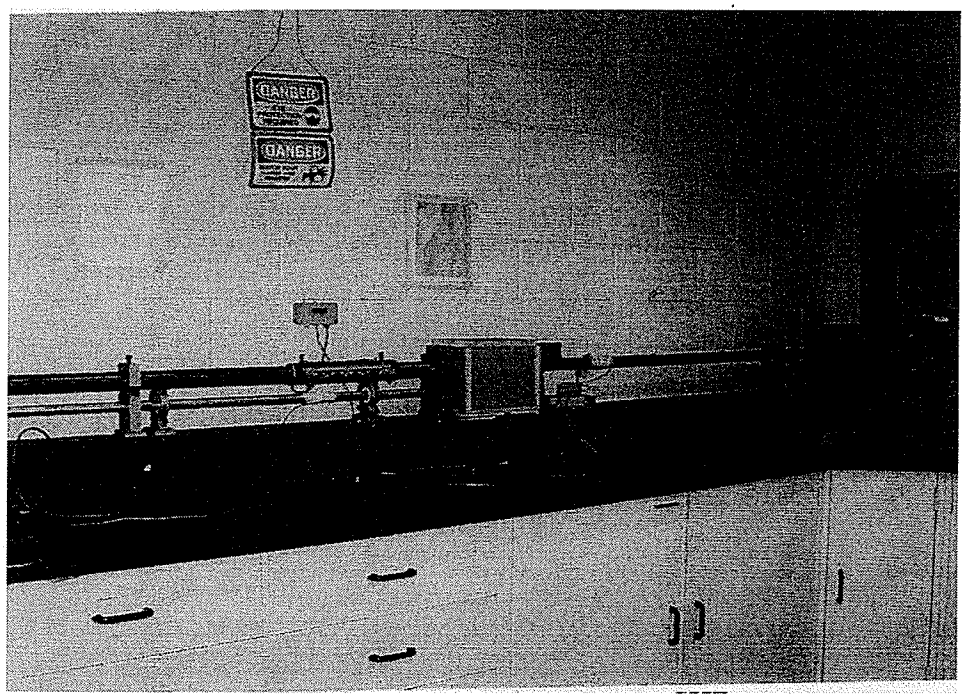

Fig 3.8: Firing barrel of SHB

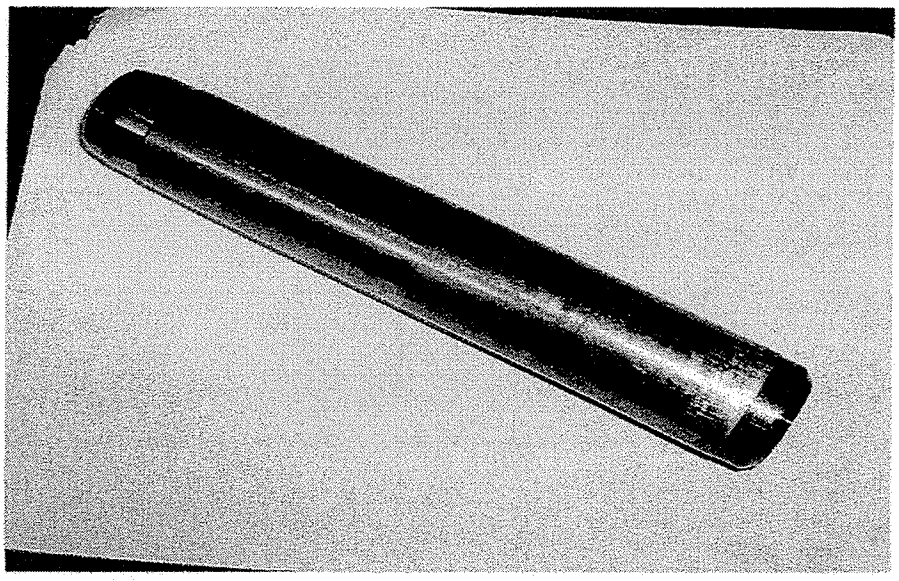

Fig 3.9: Steel Projectile used in SHB experiment

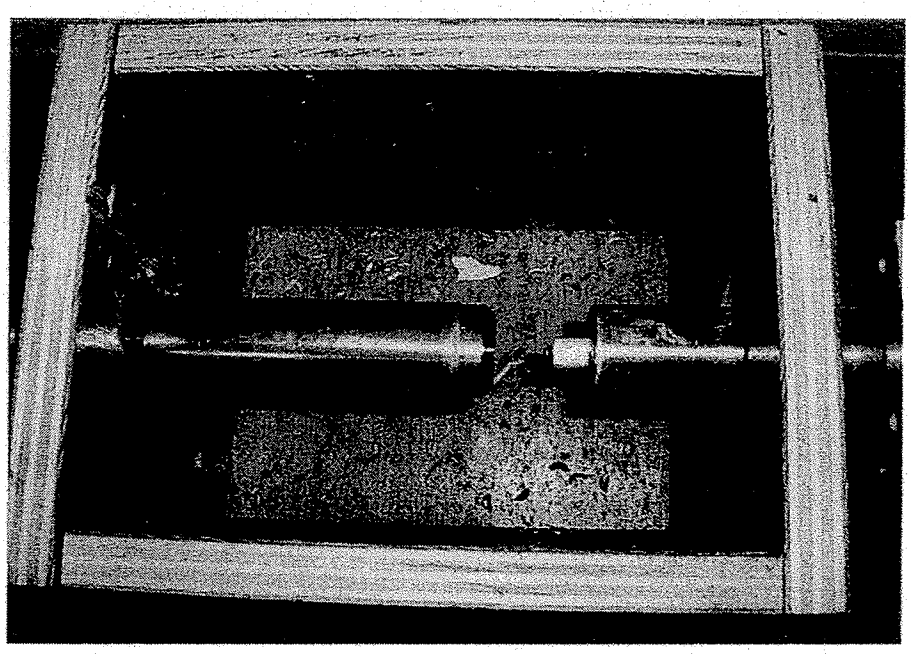

Fig3.10: Projectile left impacting the specimen mounted on the transmitted bar

The signal from the transmitted bar was collected by the oscilloscope in form of voltage–time data. Equipment calibration shows that the relationship between load and recorded signal voltage is given as follows:

$$\text{Load (KN)} = \text{Voltage (mV)} * 0.1601 \qquad (3.1)$$

Assuming constant volume, linear variation of displacement with time and constant strain rate, the true stress and true strain at time are given by the following expressions:

$$\varepsilon(t_s) = \text{In}\frac{L_i}{L_i - (L_i - L_f)(t_s / t_f)} \qquad (3.2)$$

$$\sigma(t_s) = \frac{P_{(t_s)}}{A_i}\frac{L_i - (L_i - L_f)(t_s / t_f)}{L_i} \qquad (3.3)$$

where L_i and L_f are the initial and final lengths of the tested specimens (Fig 3.11). The maximum strain in a specimen is directly proportional to the stain rate and the length of the striker bar.

$$\varepsilon = 2\dot{\varepsilon}\frac{l}{C_o} \quad \text{Or} \quad \dot{\varepsilon} = \frac{C_o}{2l}\varepsilon \qquad (3.4)$$

Where C_o is the longitudinal wave propagation velocity in the transmitted bar. The strain rates were calculated for each sample using equation 3.4 and are shown in Table3.1. Dynamic stress strain curves at high strain rates were generated using equation 3.2-3.4 and are shown in Table3.1.

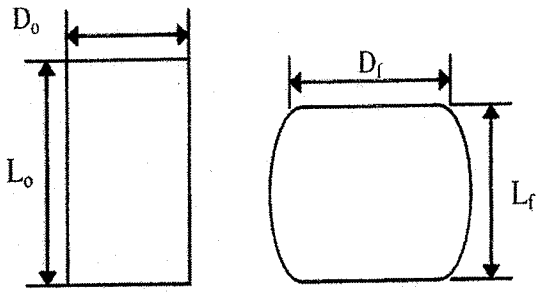

Fig 3.11: Change in geometry of the specimen during testing

Table3.1: experimental data sheet for high strain –rate testing

Sample No	Material	Lo (mm)	Do (mm)	Area (mm^2)	Pres-sure (kPa)	Time (s)	Lf	Impact velocity (m/s)	Impact Momen-tum (kg.m/s)	Nominal Strain	Strain Rate (/s)
S. 1	RHA Steel	10.46	9.39	69.3	180	12.73	7.52	21.60	41.95	0.281	2818
S. 2	RHA Steel	10.49	9.39	69.3	200	12.03	7.29	22.86	44.39	0.305	3059
S. 3	RHA Steel	10.48	9.43	69.9	200	11.99	7.20	22.94	44.54	0.313	3138
S. 4	RHA Steel	10.66	9.46	70.3	220	11.47	6.96	23.98	46.56	0.347	3480
S. 5	RHA Steel	10.75	9.43	69.9	240	11.10	6.78	24.77	48.11	0.369	3703
S. 6	RHA Steel	10.54	9.35	68.7	280	10.24	6.12	26.86	52.16	0.419	4205
S. 7	RHA Steel	10.61	9.47	70.5	320	9.48	5.43	29.01	56.33	0.488	4895
S. 8	RHA Steel	10.51	9.39	69.3	340	9.26	5.37	29.70	57.68	0.489	4904
S. 9	RHA Steel	10.68	9.48	70.6	360	9.01	3.50	30.52	59.27	0.663	6741
S.10	RHA Steel	10.68	9.5	70.9	360	9.00	3.48	30.56	59.34	0.674	6759
S.11	RHA Steel	10.68	9.48	70.6	360	9.00	3.60	30.56	59.34	0.663	6649
S.12	RHA Steel	10.68	9.45	70.2	400	8.60	3.40	31.98	62.10	0.682	6835
Al. 1	Aluminum	10.65	9.41	69.6	200	11.74	2.42	23.42	45.49	0.770	7748
Al. 2	Aluminum	10.54	9.43	69.9	180	12.29	2.48	22.38	43.45	0.760	7667
Al. 3	Aluminum	10.66	9.45	70.2	140	14.23	3.64	19.33	37.53	0.650	6603
Al. 4	Aluminum	10.6	9.46	70.3	100	16.23	4.68	16.94	32.91	0.550	5600
Al. 5	Aluminum	10.55	9.42	69.7	100	16.18	4.54	14.82	28.79	0.440	4427
Al. 6	Aluminum	10.6	9.42	69.7	80	18.55	5.92	14.75	28.63	0.430	4386
Al. 7	Aluminum	10.63	9.33	68.4	80	18.65	5.98	19.98	29.09	0.460	4632
Al. 8	Aluminum	10.65	9.39	69.3	80	18.36	5.73	17.00	33.01	0.560	5712
Al. 9	Aluminum	10.4	9.49	70.8	200	11.74	2.44	23.42	45.49	0.760	7674
Al. 10	Aluminum	10.5	9.48	70.6	180	12.40	2.76	22.18	43.07	0.730	7391
Al. 11	Aluminum	10.48	9.5	70.9	180	12.34	2.68	22.29	43.28	0.740	7462
Al. 12	Aluminum	10.58	9.5	70.9	180	12.40	3.18	22.18	43.07	0.690	7013
Al. 13	Aluminum	10.5	9.5	70.9	180	12.45	2.80	22.09	42.89	0.730	7353
Al. 14	Aluminum	10.6	9.46	70.3	150	13.30	3.33	20.68	40.16	0.680	6877
Al. 15	Aluminum	10.62	9.5	70.9	150	13.33	3.38	20.63	40.07	0.680	6835
Al. 16	Aluminum	10.5	9.5	70.9	150	13.32	3.64	20.65	40.10	0.650	6551
Al. 17	Aluminum	10.5	9.5	70.9	150	13.27	3.38	20.72	40.24	0.670	6799
Al. 18	Aluminum	10.52	9.54	71.5	150	13.34	3.50	20.61	40.04	0.660	6691
Al. 19	Aluminum	10.6	9.5	70.9	150	13.34	3.42	20.61	40.04	0.670	6792
Al. 20	Aluminum	10.54	9.52	71.2	150	13.29	3.36	20.69	40.19	0.680	6830
Al. 21	Aluminum	10.5	9.52	71.2	180	12.38	2.92	22.21	43.14	0.720	7238
Al. 22	Aluminum	10.53	9.5	70.9	180	12.43	3.03	22.12	42.96	0.710	7141
Al. 23	Aluminum	10.6	9.5	70.9	180	12.45	3.20	22.09	42.89	0.690	7000
Al. 24	Aluminum	10.6	9.5	70.9	200	11.58	2.76	23.21	45.07	0.730	7416
Tu. 1	Tungsten	10.44	9.52	71.2	200	12.14	8.43	22.65	43.99	0.193	1930
Tu. 2	Tungsten	10.53	9.47	70.5	220	11.77	8.33	23.36	45.38	0.209	2095
Tu. 3	Tungsten	10.6	9.66	73.3	240	11.17	8.15	24.62	47.81	0.231	2317
Tu. 4	Tungsten	10.52	9.56	71.8	280	10.36	7.64	26.54	51.55	0.274	2745
Tu. 5	Tungsten	10.52	9.57	71.9	320	9.65	7.10	28.50	55.34	0.325	3260
Tu. 6	Tungsten	10.5	9.62	72.7	340	9.38	6.87	29.32	56.93	0.346	3466

3.5 Metallurgical preparation of the materials

After using the HPB to generate high strain rate in the material, the impacted specimens were mounted using bakelite black phenolic powder, followed by grinding, polishing, and etching in preparation for metallographic investigation.

- **Mounting**

Mounting thickness is very important because very thick samples are hard to keep flat during grinding and very thin samples are hard to handle. The molding powder is black phenolic powder and the mounting temperature and pressure were 130°C and 4.2 MPa respectively. Mounting requires pressure and high temperature to fuse the powder material in to a solid mass around the sample. The elevated temperature and pressure inside the chamber allows compacting and melting the black bakelite around the samples forming a cylindrical plastic mount.(Fig 3.12)

- **Grinding and polishing**

The samples were ground on emery paper with sizes starting from 120 microns to 600 microns. After grinding the samples were polished to a mirror finished surface. The samples were polished on the 6 microns wheel first followed by the 1 micron polishing

- **Etching**

The etchants used in this study and the etching time are as listed below

- RHA Steel: 2% Nital for a bout 60 seconds
- Aluminum 5083 H131: 10ml of H_3PO_4 with 90 ml of water for about 35 seconds
- Tungsten: Murakami reagent (10g of $K_3Fe(CN)_6$, 10g of KOH and 10 ml of water) for about 60 seconds

After etching, the samples were rinsed with water and later with alcohol, dried and stored in desiccators to preserve the prepared surfaces from moisture and scratches prior to microscopic examination. All prepared samples were investigated using Zeiss optical microscope with the Clemex Vision Analyzer. Some samples were also evaluated using JELO JSM-5900 LV Scanning Electron Microscope (SEM) using applied voltage of 20V.

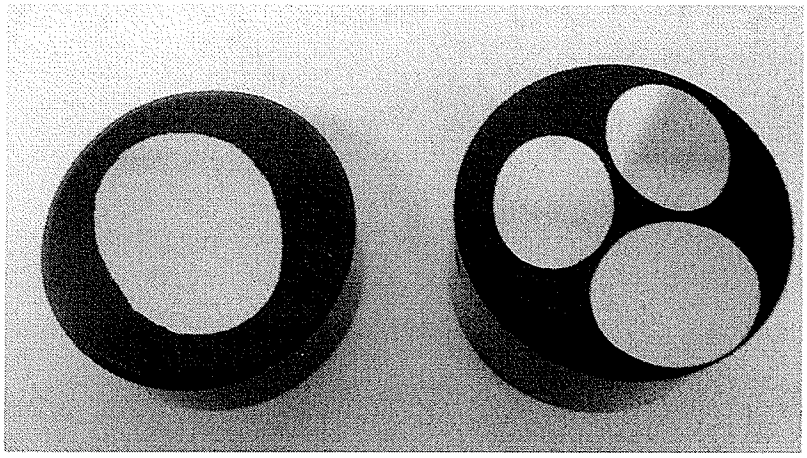

Fig: 3.12: Mounted specimen –radial section (Mag. X1.5)

3.6 Micro-hardness Measurements

The micro-hardness test was based on the Vickers method (VH). The equipment used was Letz Wetzler Micro-hardness tester. A 136° pyramids diamond indenter was used to form a square indent inside and outside the shear bands. A 50 gm load was used to form the indent depending on the metal hardness. After removing the indenter, the lengths of the two diagonals using microscopic lens guided by a small ruler were measured. By using standard hardness tables, the corresponding hardness values were determined. Hardness measurements were taken inside and outside the shear band regions in the tested samples after high velocity impact (Fig 3.13).

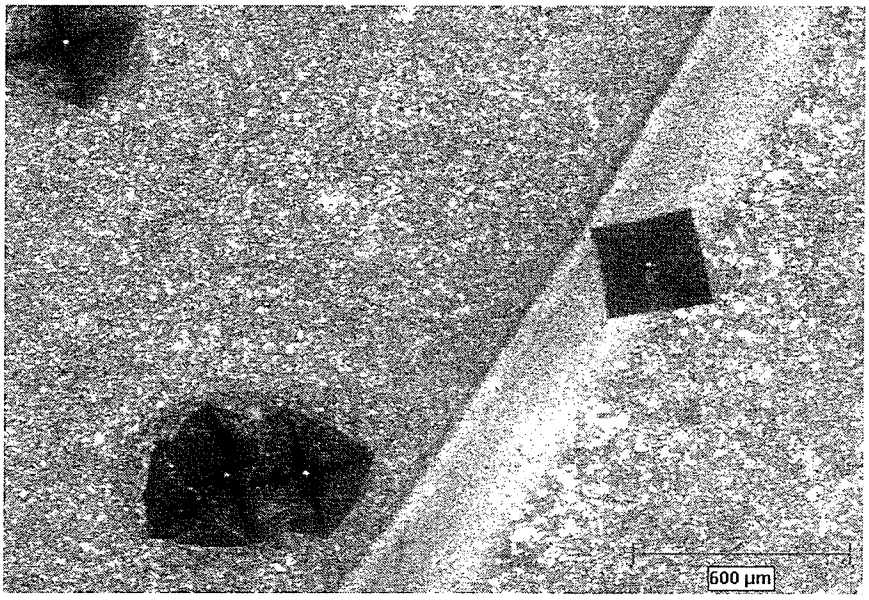

Fig 3.13: Micrograph showing indents inside of shear bands

4 CHAPTER 4: RESULTS AND DISCUSSION

4.1 Introduction

This section will cover:

1. The results of the dynamic stress-strain response for:
    - RHA Steel
    - Aluminum 5083 H131
    - Tungsten A90S
2. The behavior of the specimens and the formation of ASBs under different values of impact momentum.
3. Discussion regarding hardness of the materials both inside and outside the shear bands for each group of samples.
4. Comparison of the results from the mechanical tests and microstructural evaluation.

4.2 Dynamic stress- strain curves

Experimental data for the investigations on the RHA steel are presented in Table3.1. Typical stress strain curves obtained from high strain-rate testing of the RHA steel are presented in Fig 4.1. As the impact momentum increases from 42 Kg.m/s to 52.2 Kg.m/s the maximum flow stress increases from approximately 1200 MPa to 1450 MPa, as shown in Fig 4.1. It is also seen that the maximum flow stress then starting to go down to approximately 830 MPa as the impact momentum increases from 56.3 Kg.m/s to 59.3 Kg.m/s.

Table3.1 also gives the experimental data for the high velocity impact test on the tungsten alloy testing, while typical stress strain curves obtained are presented in Fig 4.2. According to Fig 4.3 as the impact momentum increases from 45.4 Kg.m/s to 56.9 Kg.m/s, the maximum flow stress increases from approximately 1220 MPa to 1375 MPa. The maximum flow stress then starts to decrease to approximately 1000 MPa as shown in Fig 4.2.

Table 3.1 also shows the experimental data for the high velocity impact of the test specimens for the aluminum alloy. Fig 4.3 shows the comparison of the stress vs. strain curves for five different aluminum alloys under different impact momentums during the high strain rate testing. It is obvious that impact momentum does not have significant effect on the maximum flow stress on aluminum alloys.

Fig 4.4 and 4.5 show the comparison of the curves strain rates vs. impact momentums and engineering strains vs. impact momentums respectively. It is seen that the as the impact momentum increases, strain rate and total engineering strain also increases. Fig 4.6 shows the comparison of the maximum flow vs. impact momentum for

steel, aluminum and tungsten. It is obvious from Fig 4.6 that for steel and tungsten the maximum flow stress increases initially with increase of the impact momentum and then starts to go down with further increases in impact momentum. Fig 4.7 shows the dynamic stress strain curves of all the three alloys in compression at the comparable impact momentum of a bout 45 Kg.m/s. Detailed description of the curves will be discussed in section 4.5.

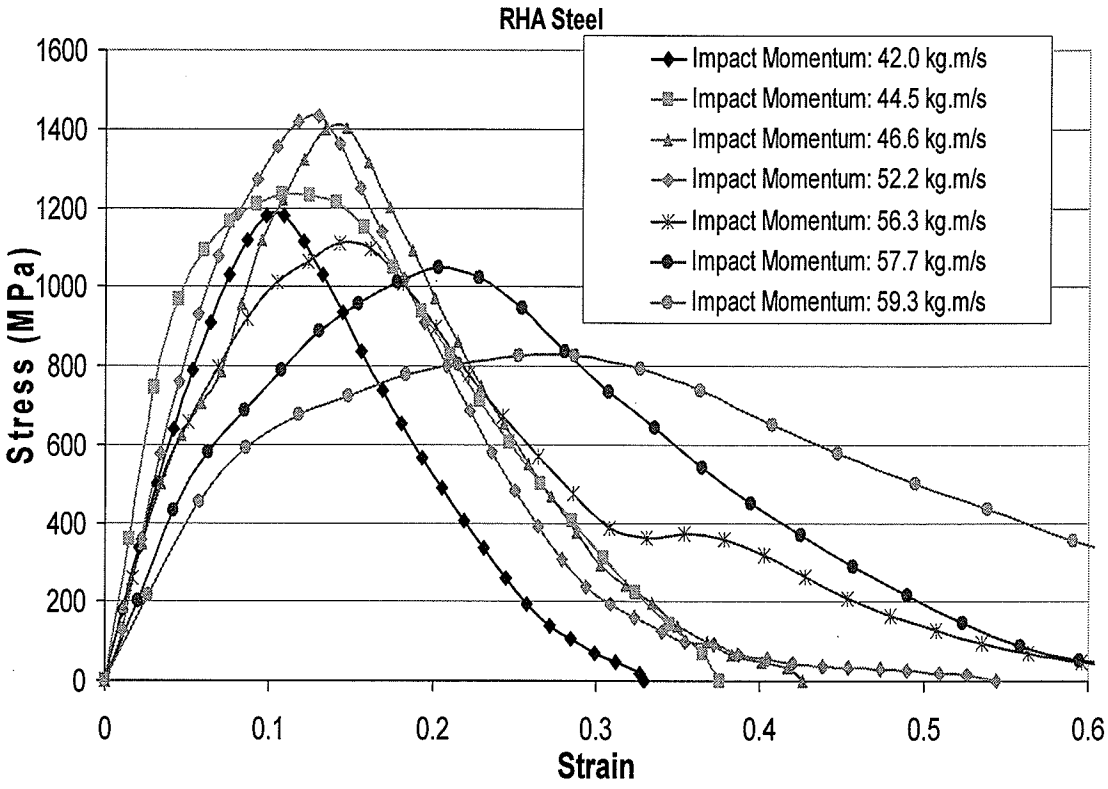

Fig 4.1: Dynamic stress-strain curves for RHA steel samples under different impact momentum (The curves are given in color to enable distinction between specimens)

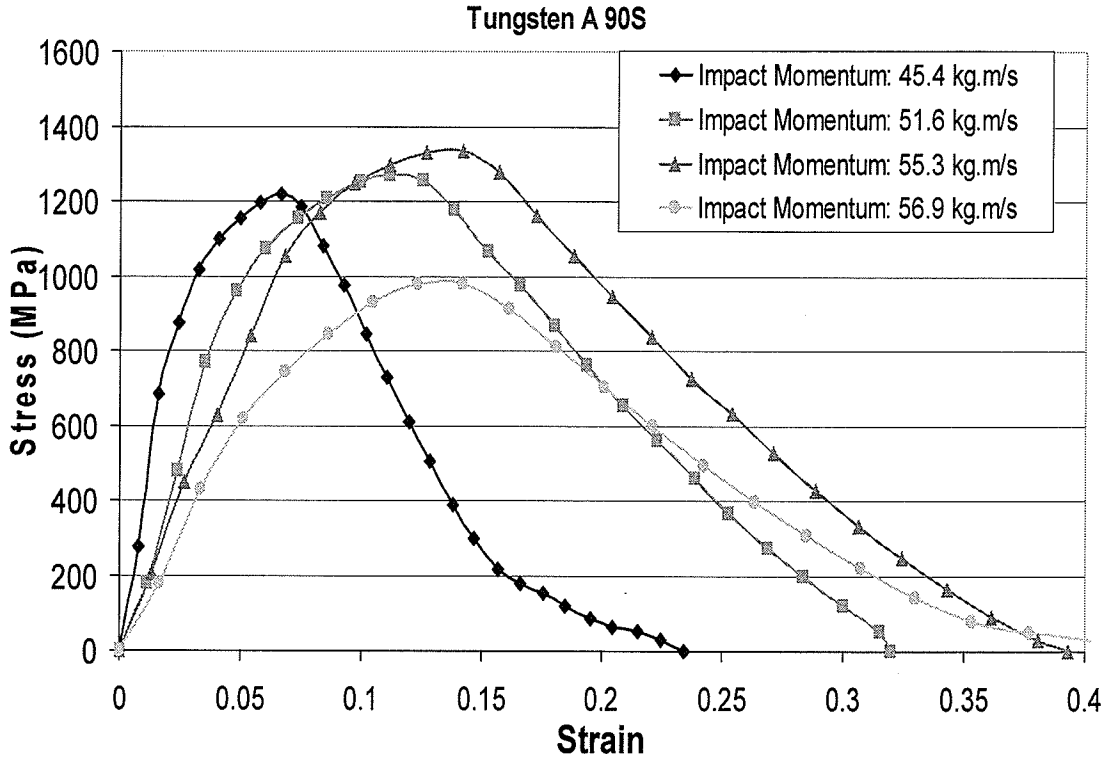

Fig 4.2: Dynamic stress-strain curves for Tungsten samples under different impact momentum (The curves are given in color to enable distinction between specimens)

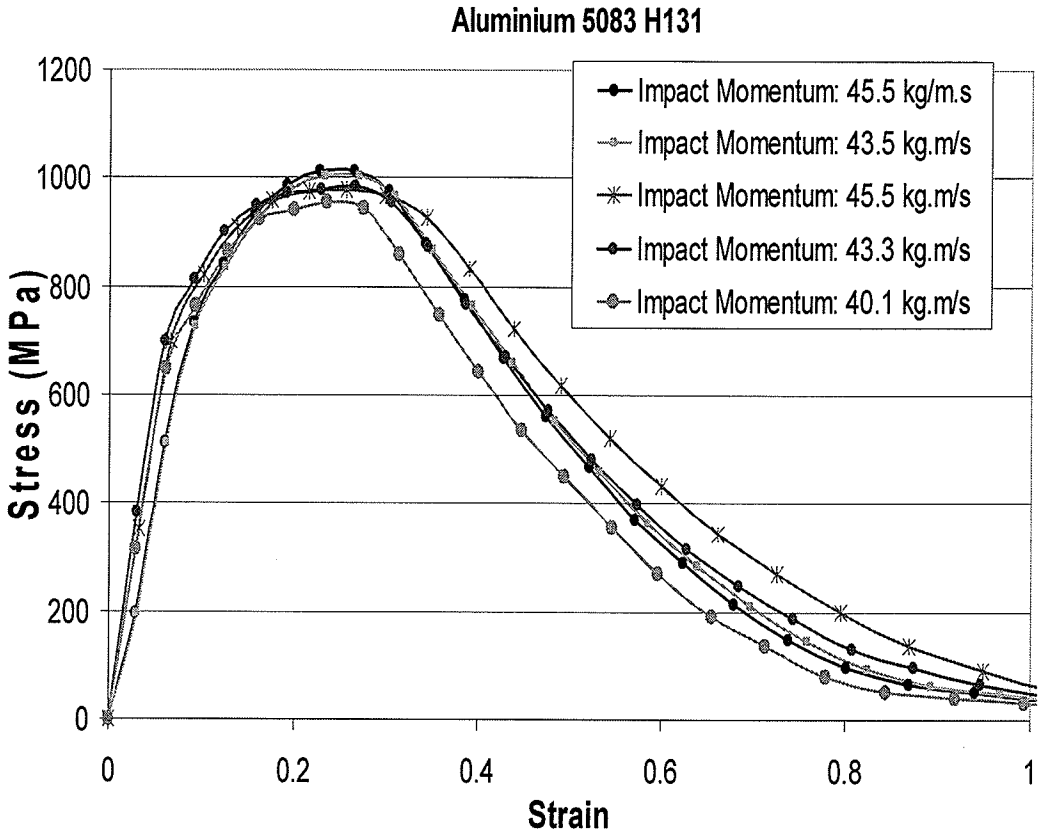

Fig 4.3: Dynamic stress-strain curves for Aluminum samples under different impact momentum (The curves are given in color to enable distinction between specimens)

4.3 Comparison of the curves for Steel, Aluminum and Tungsten

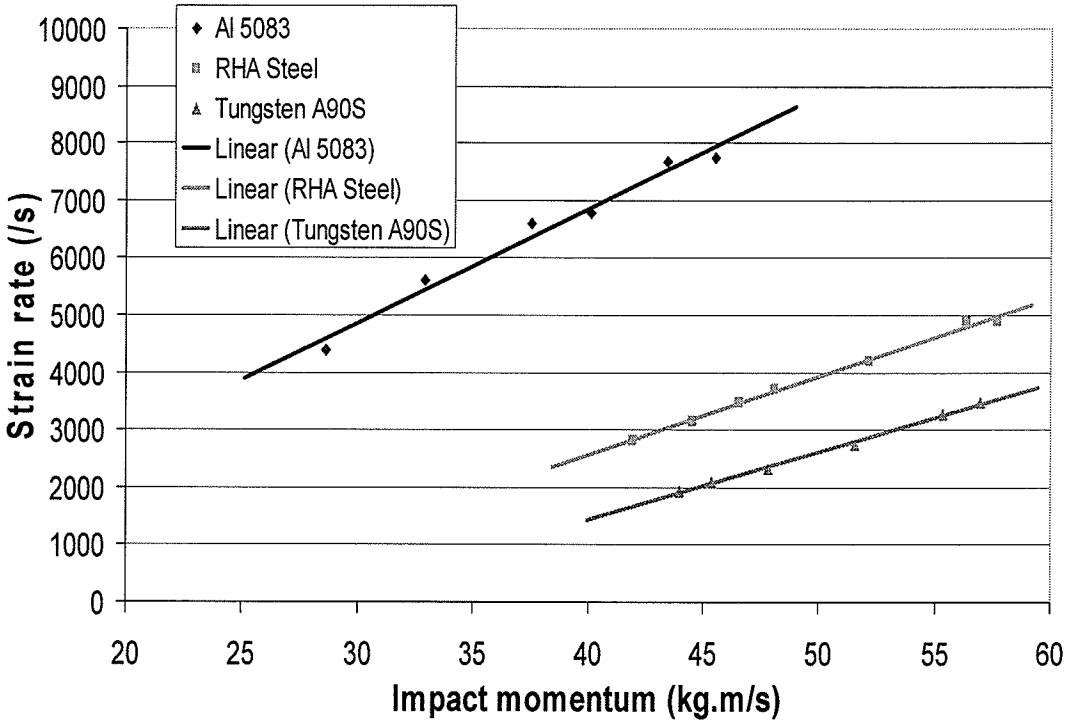

Fig 4.4: Effect of impact momentum on strain rates (The curves are given in color to enable distinction between specimens)

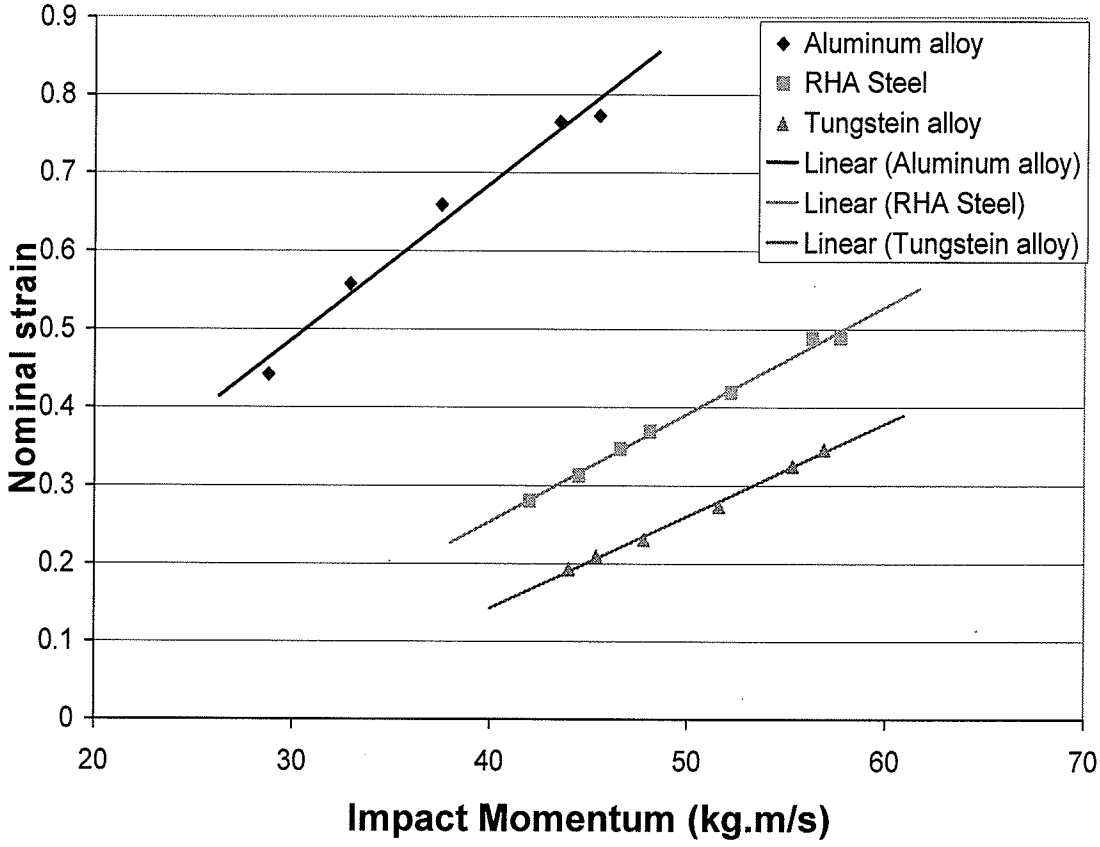

Fig 4.5: The effect of impact momentum on total engineering strain (The curves are given in color to enable distinction between specimens)

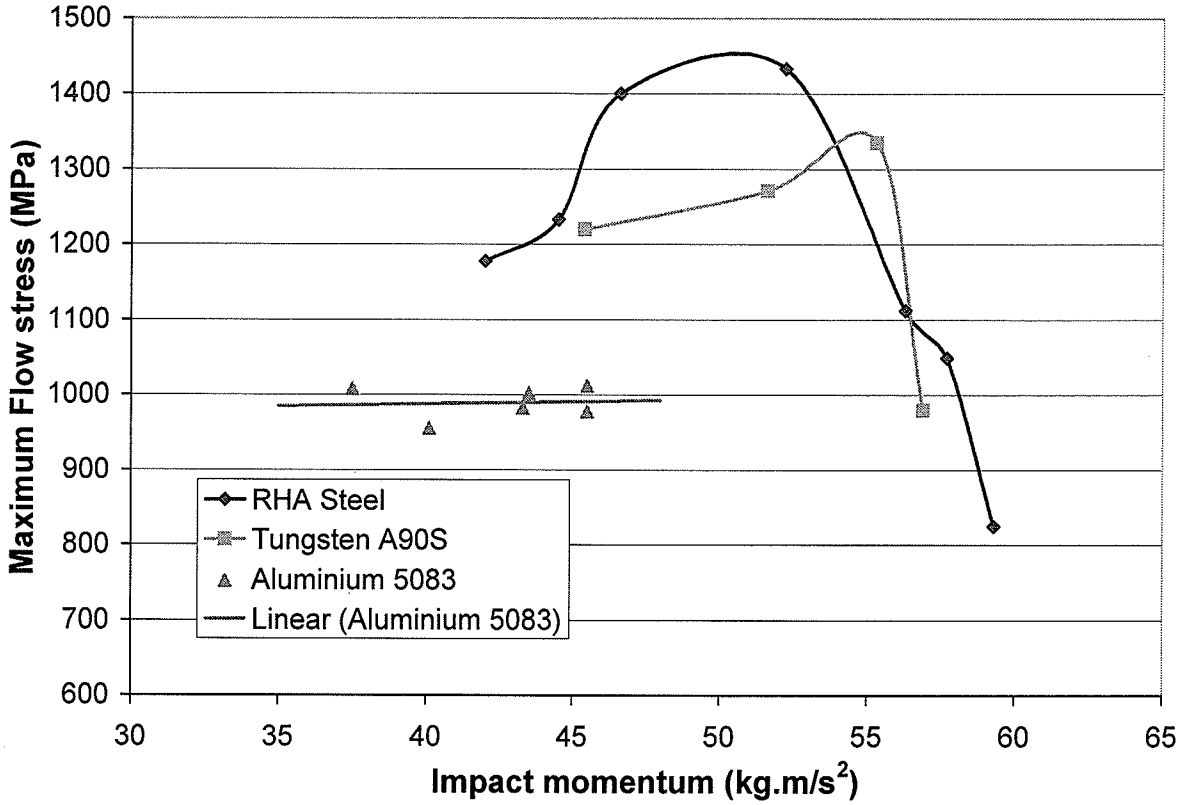

Fig 4.6: Effect of impact momentum on maximum flow stress (The curves are given in color to enable distinction between specimens)

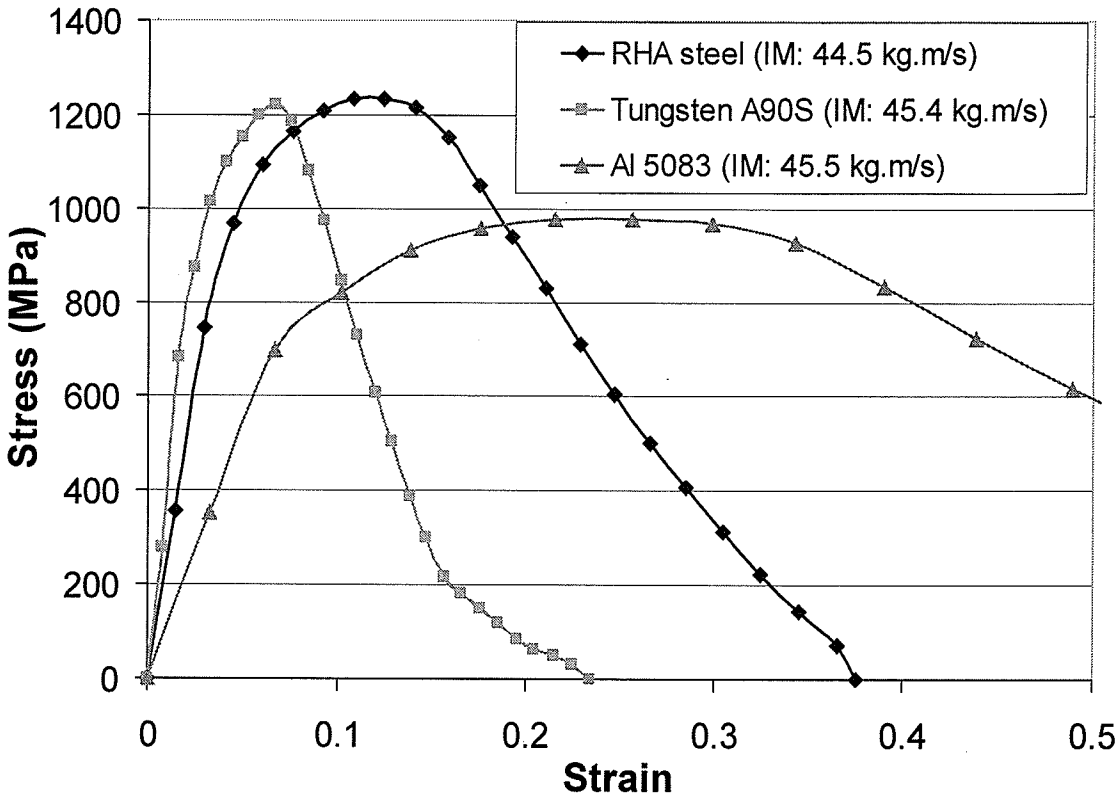

Fig 4.7: Dynamic stress strain curves of all the three alloys in compression at comparable impact momentum of about 4 5 kg.m/s (The curves are given in color to enable distinction between specimens, sample S.3, Al.1, and Tu.2)

4.4 Optical microscopic analysis and hardness measurements

After using the SHPB to generate high strain rate in the material, the specimens were examined using optical microscopy to evaluate and compare the formation of ASBs in the samples during impact testing. The hardness of the shear band is higher than that of the bulk material because there are significant increases in dislocations within the bands [10]. Tungsten samples were also evaluated under Scanning Electron Microscopy (SEM) for further analysis.

4.4.1 Optical microscopy in steel samples

As seen from Fig 4.8 kgm/s and Fig 4.9 kgm/s, steel samples show no shear band at the impact momentum of 41.94 kgm/s and 44.53 kgm/s. With increasing the impact momentum to 46.6 kgm/s deformed bands starts to initiate at the edge of the specimens. By further increasing the impact momentum to 56.34 kgm/s, the white etching bands are observed in the steel samples. The white etching bands becomes thicker as impact momentum increases up to 59.42 kgm/s when the steel sample cannot withstand the high impact momentum and fragments. The detailed microscopy analysis of steel sample will be discussed in section 4.5.

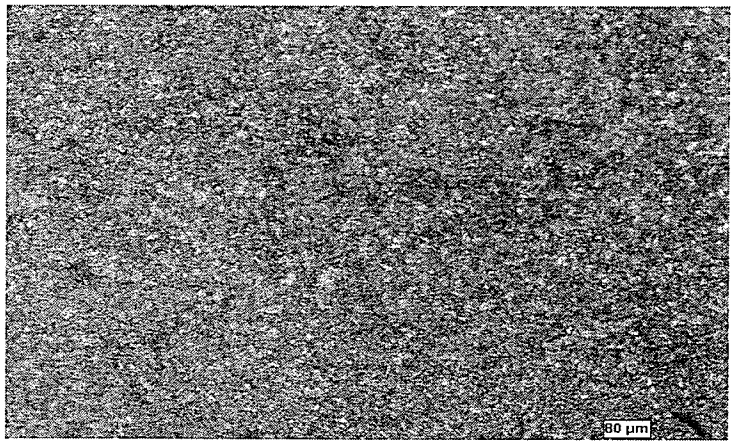

Fig 4.8: Steel sample (1) impacted at 41.94 kgm/s (no shear band)

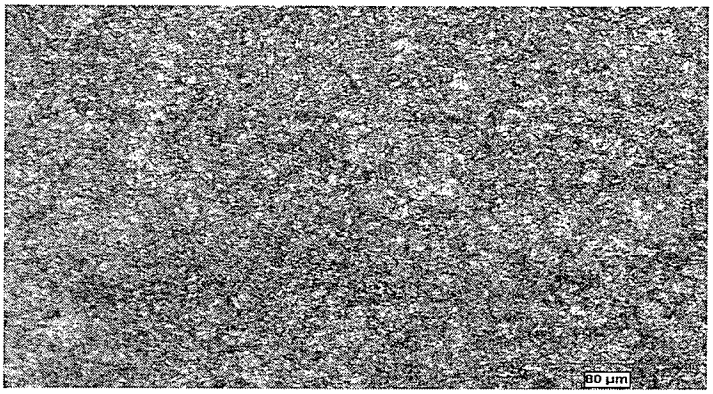

Fig 4.9: Steel sample (3) impacted at 44.53 kgm/s (no shear band)

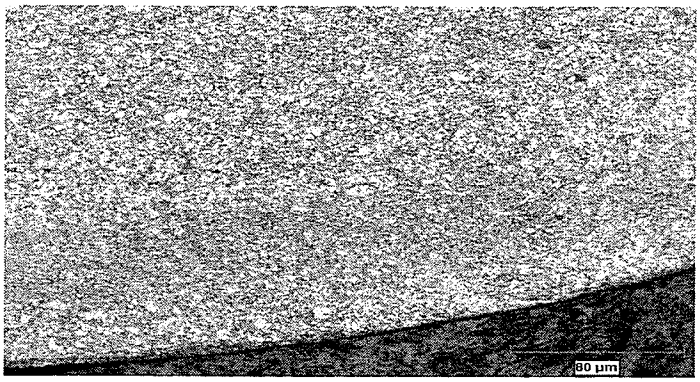

Fig 4.10: Steel sample (4) impacted at 46.6 kg.m/s (Deformed bands along the edge of the sample)

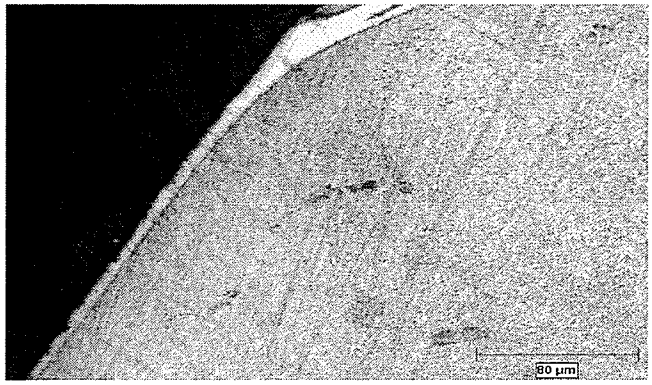

(a)

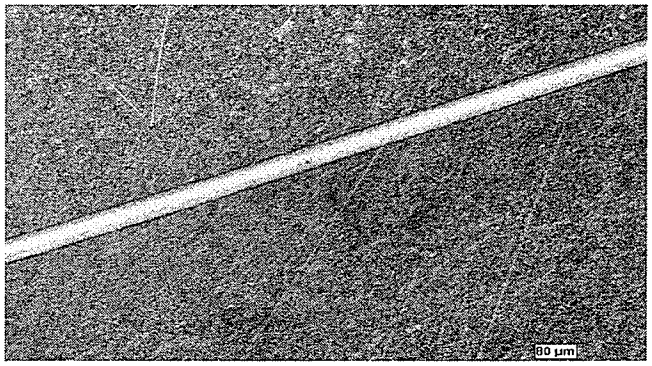

(b)

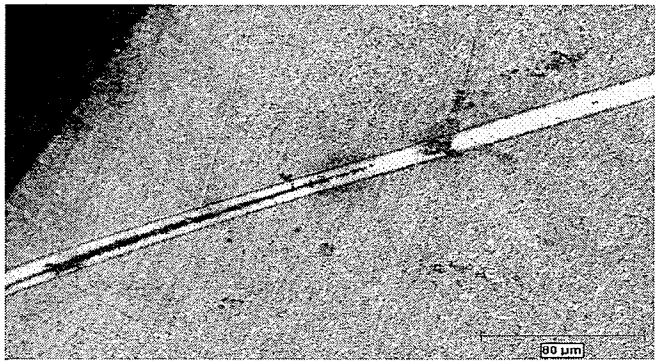

(c)

Fig 4.11: Steel sample (7) impacted at 56.34 kgm/s, (a) Start of the white etching bands, (b) Adiabatic shear band, (c) Initiation of crack within shear band

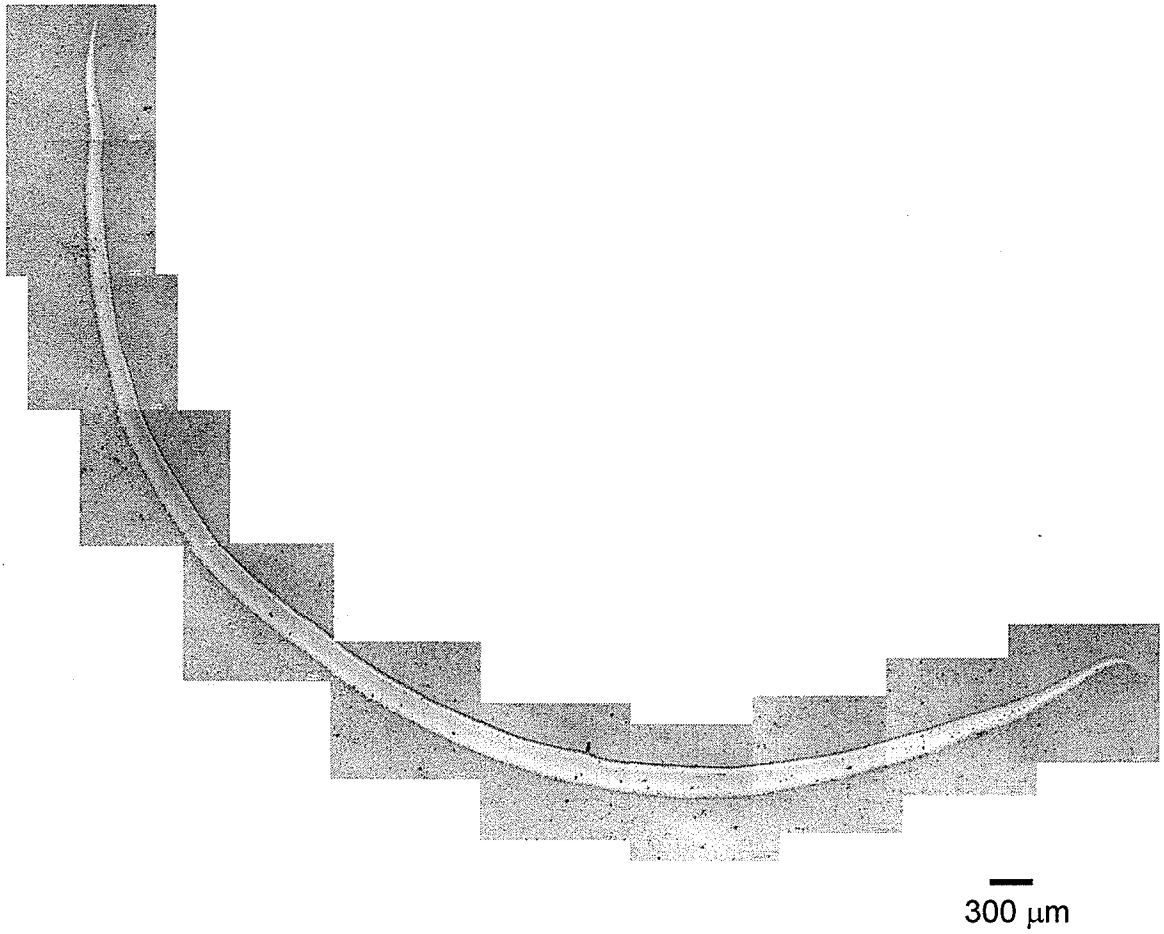

Fig 4.12: Optical micrographs showing an overview of a c-shaped adiabatic shear band (white etching band) observed on transverse section of RHA Steel subjected to an impact momentum of 56.6 kg.m/s

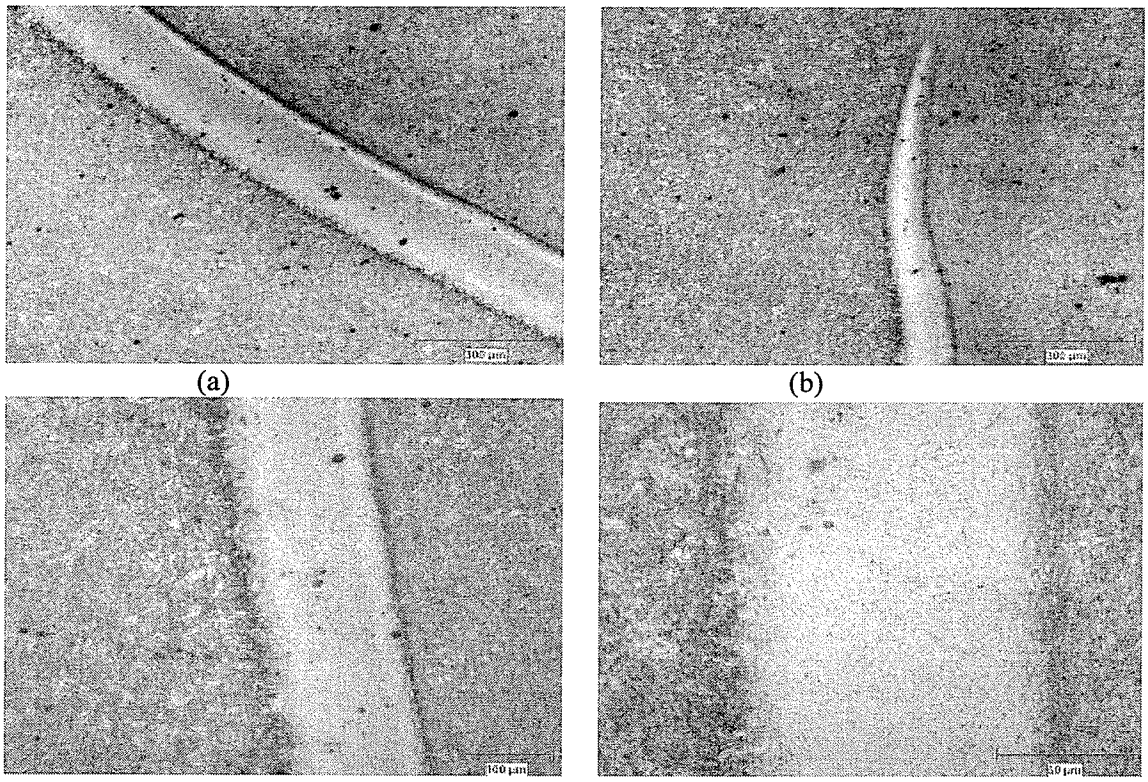

Fig 4.13: (a) Steel sample (8) shows a thicker shear band for impact momentum of 57.7 kgm/s than the previous samples that are subjected to lower impact momentum, (b) the end of the shear band in the middle of the specimen, (c) & (d) higher magnification

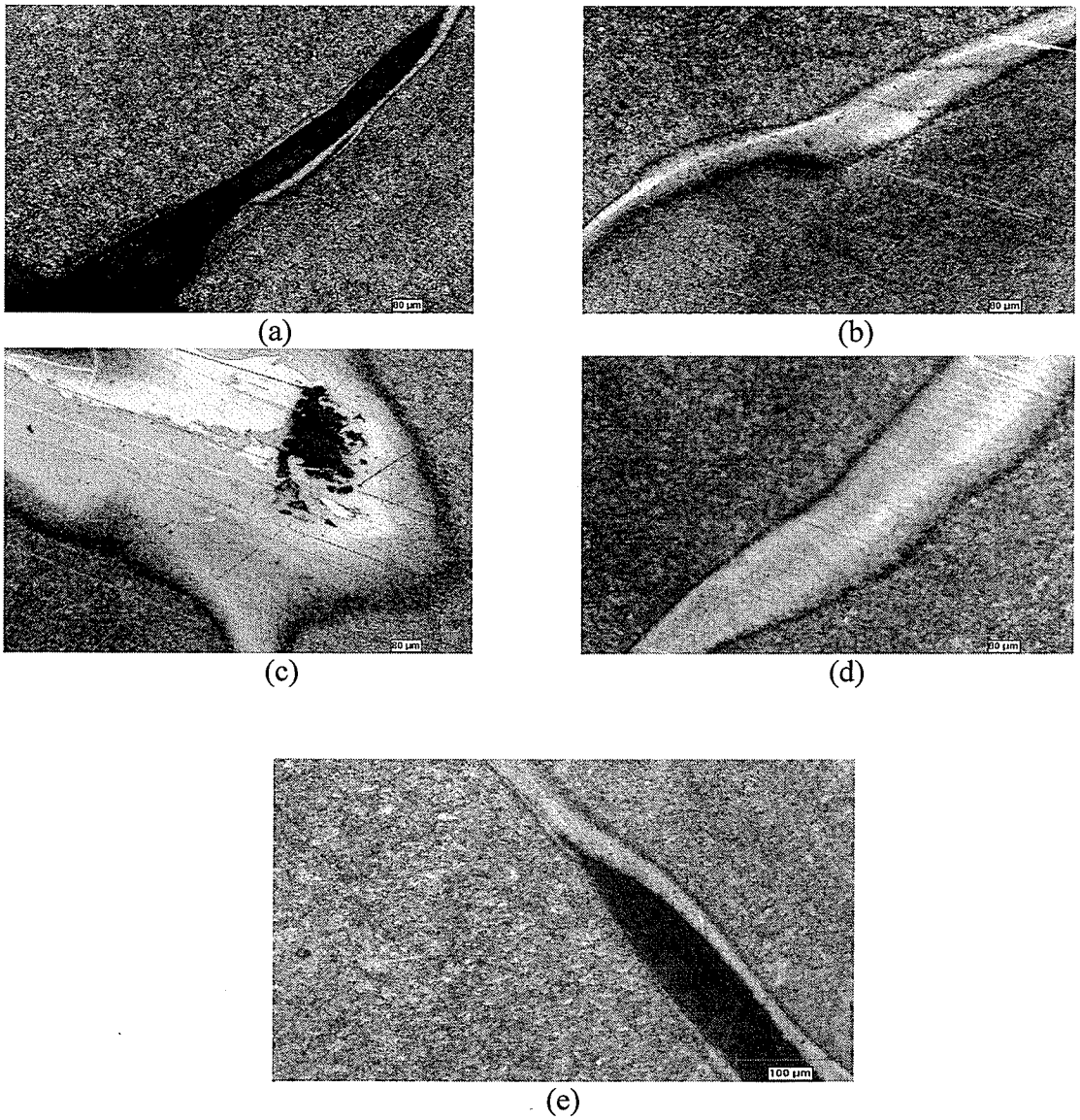

Fig 4.14: Steel sample (9) impacted at 59.42 kgm/s (a) initiation of crack, (b) shear band, (c) Splash of the shear band, (d) very thick shear band, (e) crack propagation inside shear band.

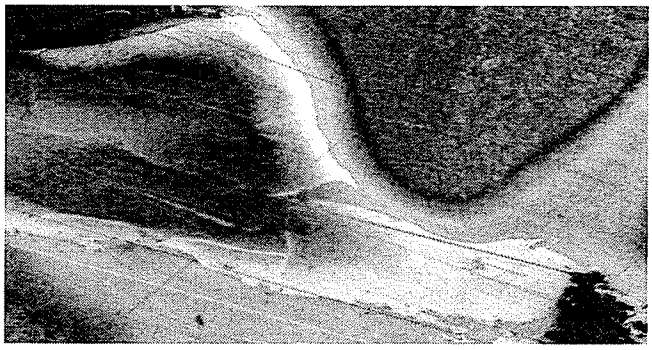

(a)

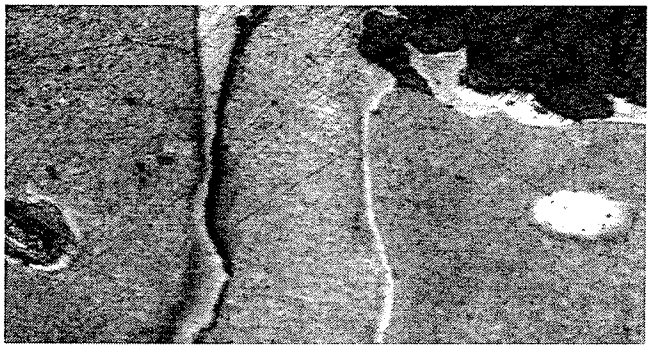

(b)

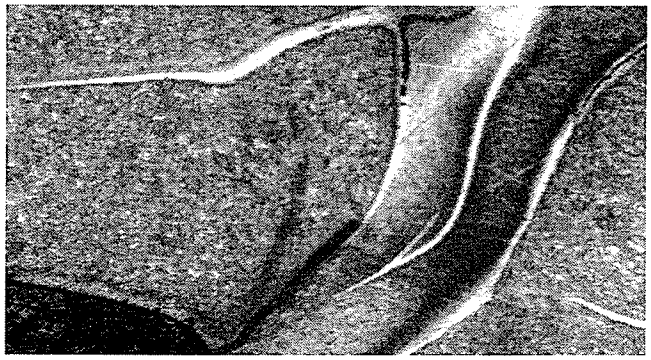

(c)

Fig 4.15: Optical micrograph showing splashing and spreading of ASBs in RHA Steel impacted at 59.3 kg.m/s

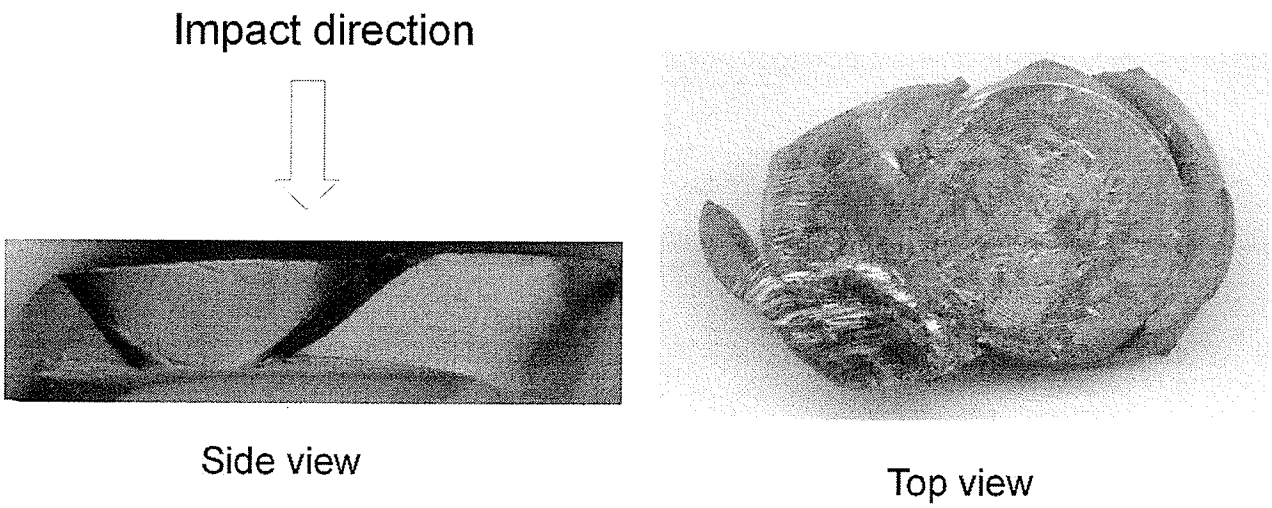

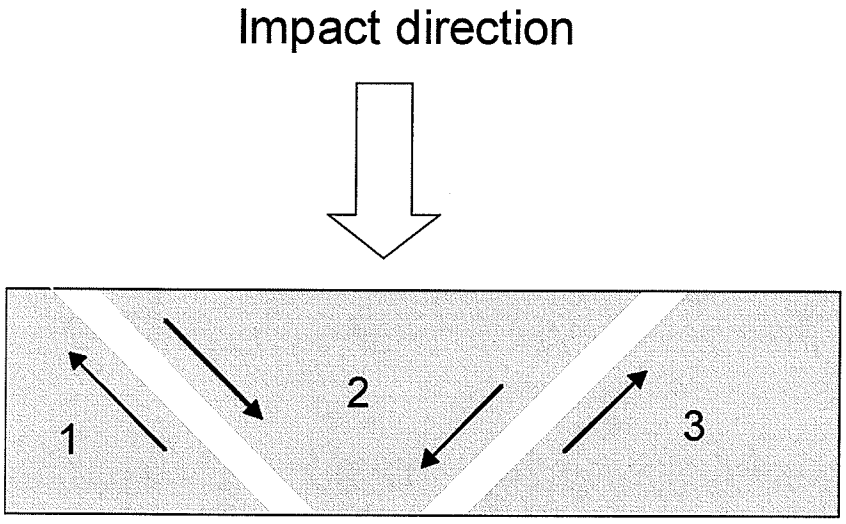

Fig 4.16: (a) Optical macrograph (Mag. X3) of the steel sample 9 (S.9) impacted at 59.3 kg.m/s showing adiabatic shear and failure fusion of fragments along the shear bands. (b) A sketch of the longitudinal section of the sample after impact showing three fragments 1, 2 and 3 fused together along the ASBs (white strips). Arrows indicate shear flow directions

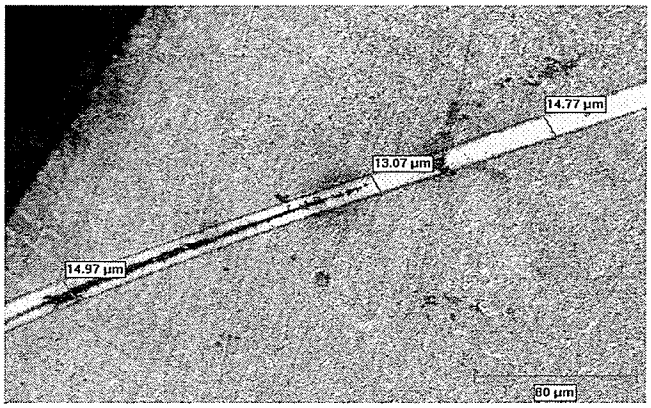

Fig 4.17: Steel Sample 7, Shear Band Width Measurement

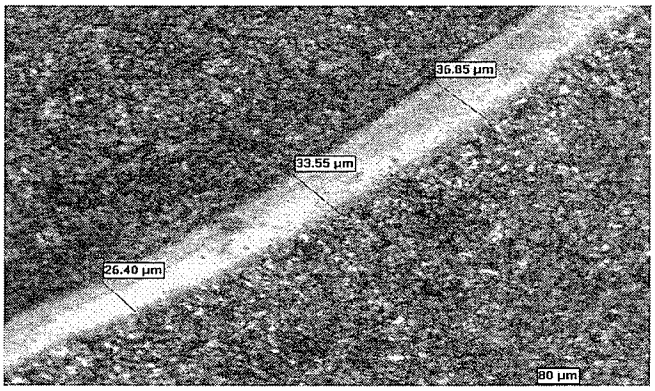

Fig 4.18: Steel Sample 8, Shear Band Width Measurement

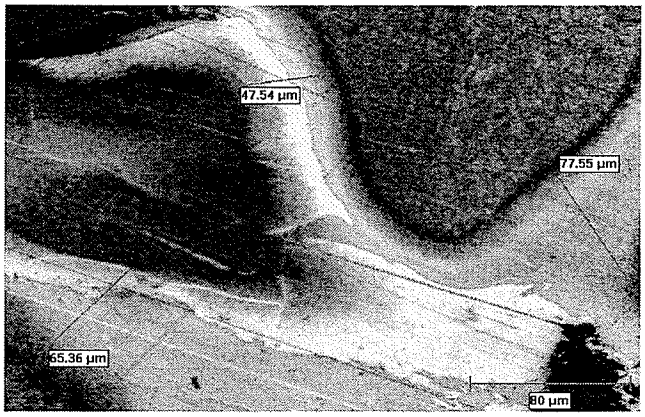

Fig 4.19: Steel Sample 9, Shear Band Width Measurement

Table 4.1: Width of the shear bands

Steel sample	Width of the shear bands	Average Width
S.7	14.77μm 13.07μm 14.97μm	14.27μm
S.8	36.85μm 33.55μm 26.4μm	32.27μm
S.9	77.55μm 47.54μm 65.36μm	63.484μm

Table 4.2: Hardness Measurements (VH) of Steel samples

Steel Samples	Average outside of the shear bands	Average inside of the shear bands
S.1	250VH	No shear Bands (NSB)
S.3	252VH	NSB
S.4	253VH	743VH
S.7	255.5VH	847VH
S.8	256VH	988VH
S.9	258VH	1355VH

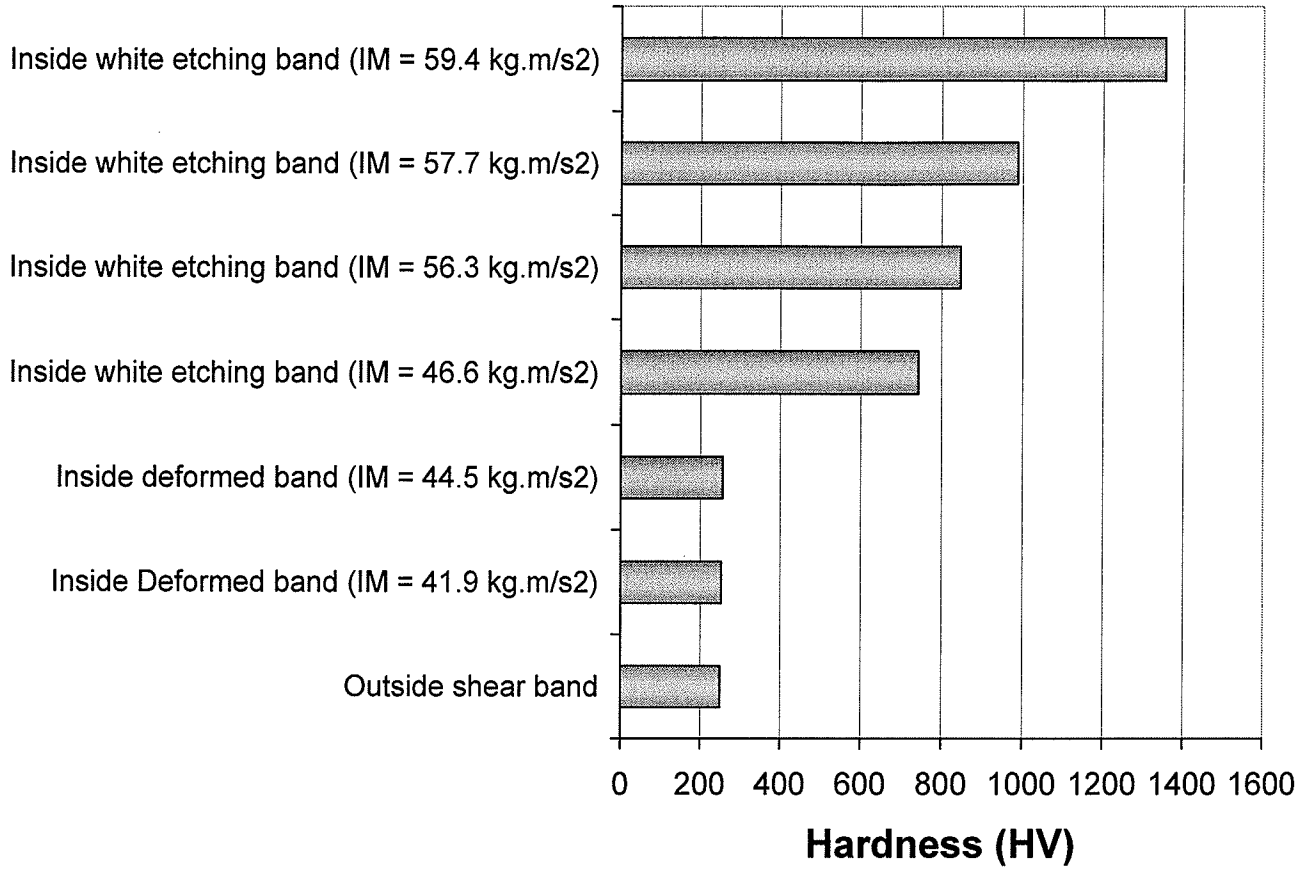

Fig 4.20: Hardness outside and inside shear bands in RHA Steel as a function of impact momentum (IM)

4.4.2 Optical microscopy in Aluminum sample

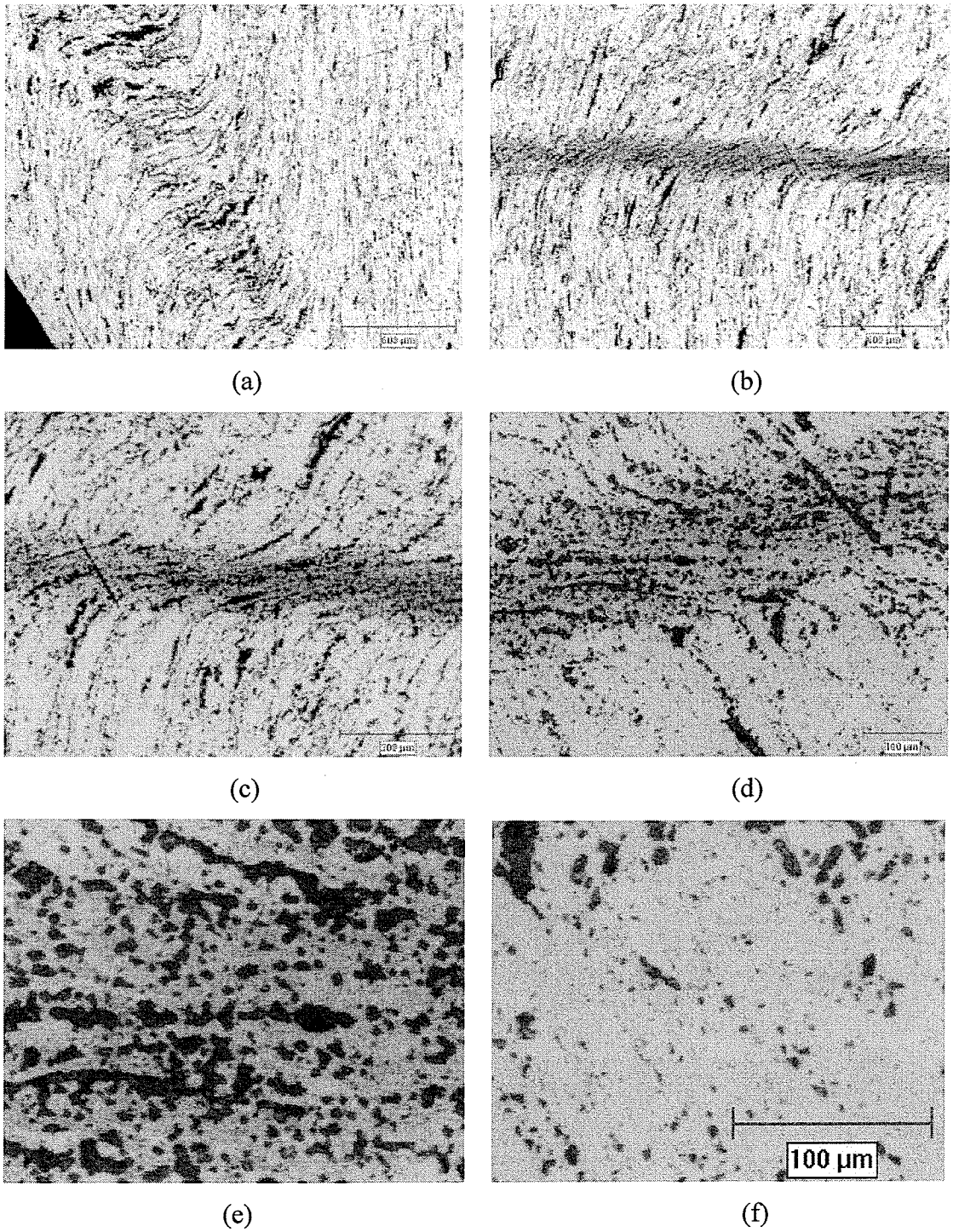

Fig 4.21: Optical micrographs showing adiabatic shear band along transverse section of Aluminum 5083 H131 alloy impacted at 29.0 kg.m/s: (a) circular ASB close to the circumference. (b), (c) & (d) linear ASB across the cross section at different magnifications. (e) Microstructure inside ASB and (f) microstructure outside ASB

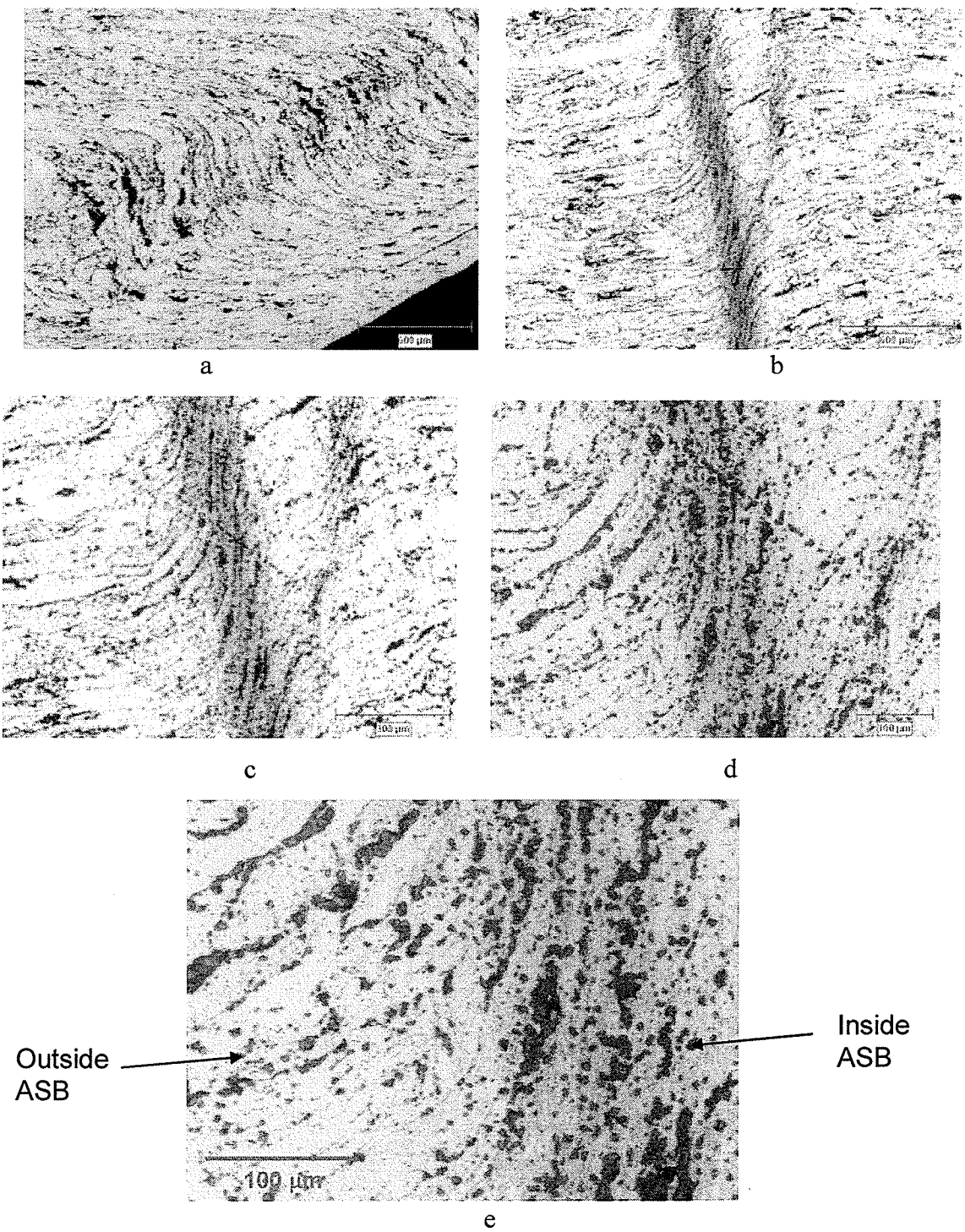

Fig 4.22: Optical micrographs showing adiabatic shear band along transverse section of Aluminum 5083 H131 alloy impacted at 40.1 kg.m/s: (a) circular ASB close to the circumference. (b), (c), (d) linear ASB across the cross section at different magnifications, (e) Microstructure inside and outside ASB

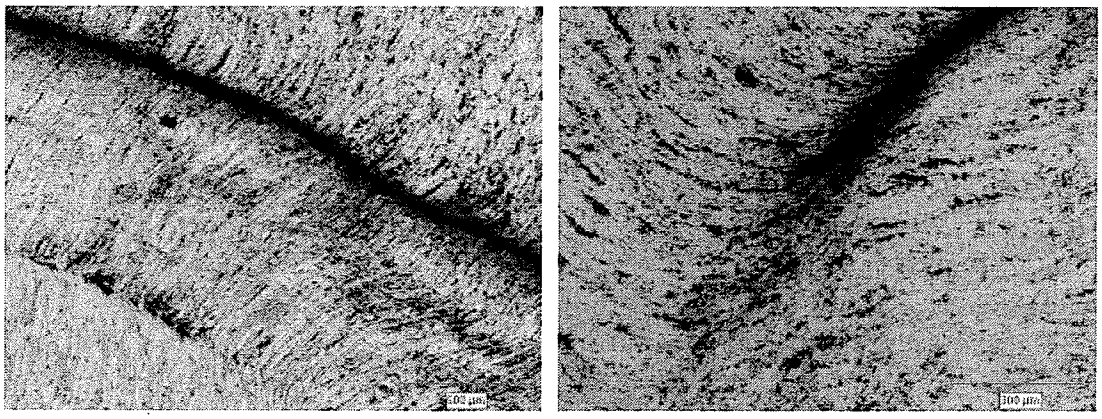

a b

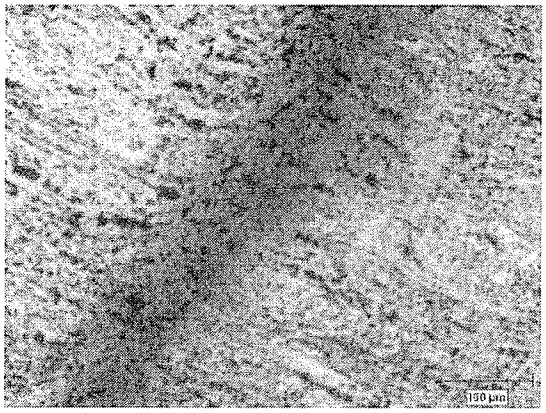

c

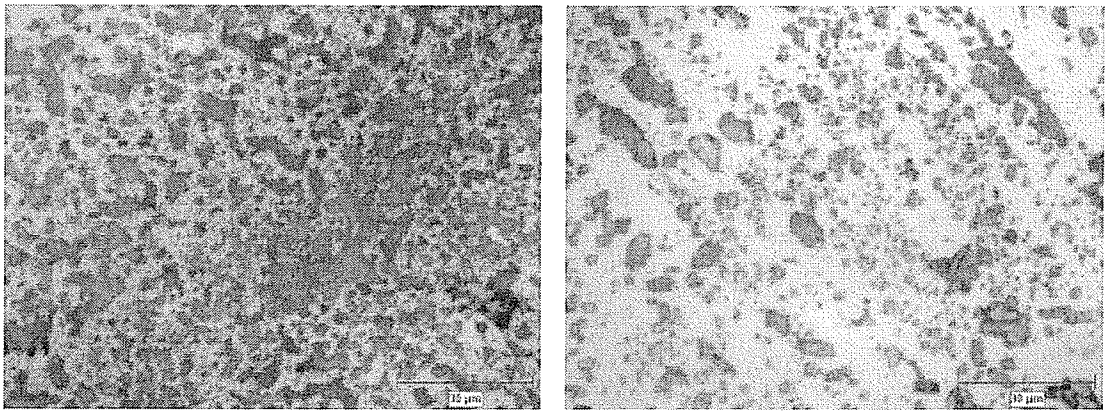

d e

Fig 4.23: Optical micrographs showing adiabatic shear band along transverse section of Aluminum 5083 H131 alloy impacted at 45.49 kg.m/s: (a) (b), (c) ASB across the cross section at different magnifications. (d) Microstructure inside ASB and (e) Microstructure outside ASB

Table 4.3: Hardness Measurements (VH) of aluminum samples

Aluminum Samples	Outside of the deformed bands(VH)	Inside of the deformed bands(VH)
Al. 1	137μm	157μm
Al. 2	127μm	154μm
Al. 3	142μm	154μm
Al. 4	131μm	158μm
Al. 5	142.5μm	155.5μm
Al. 6	127.5μm	153.5μm
Al. 7	132μm	148.5μm
Al. 8	130.5μm	142.5μm

4.4.3 Optical microscopy in Tungsten samples

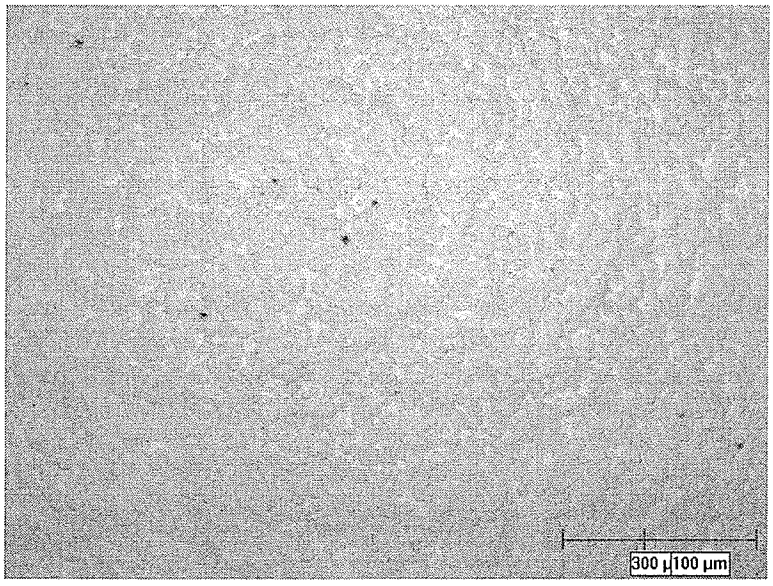

Fig 4.24: Optical micrograph showing microstructure of the Tungsten alloy

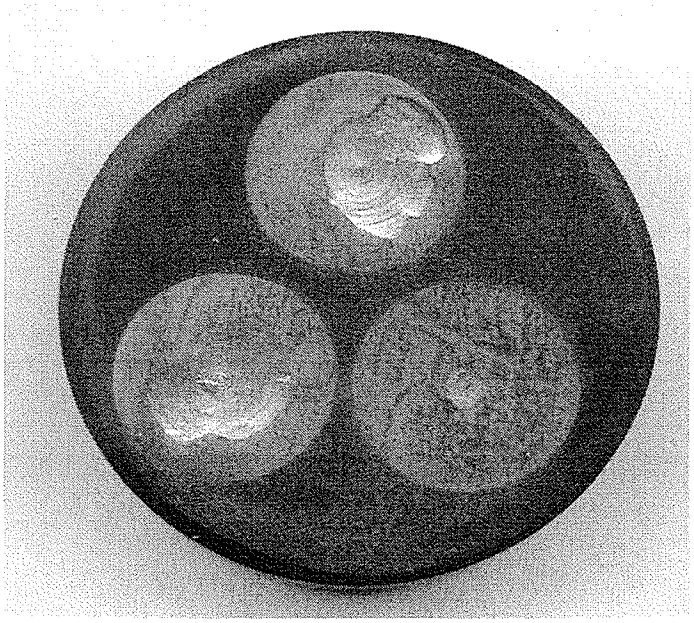

Fig 4.25: Polished surface of impacted Tungsten A90S showing small fragment during testing (Mag. X2.2)

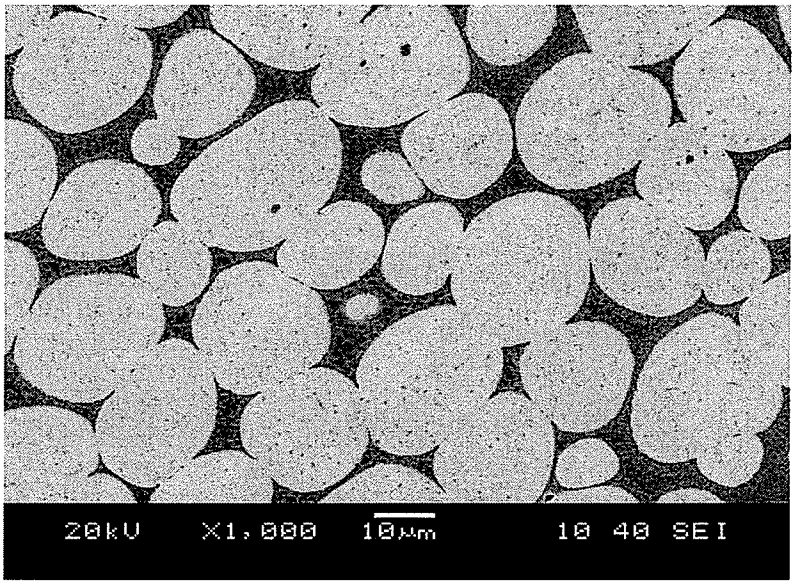

Fig 4.26: Microstructure of the Tungsten alloy- SEM micrograph

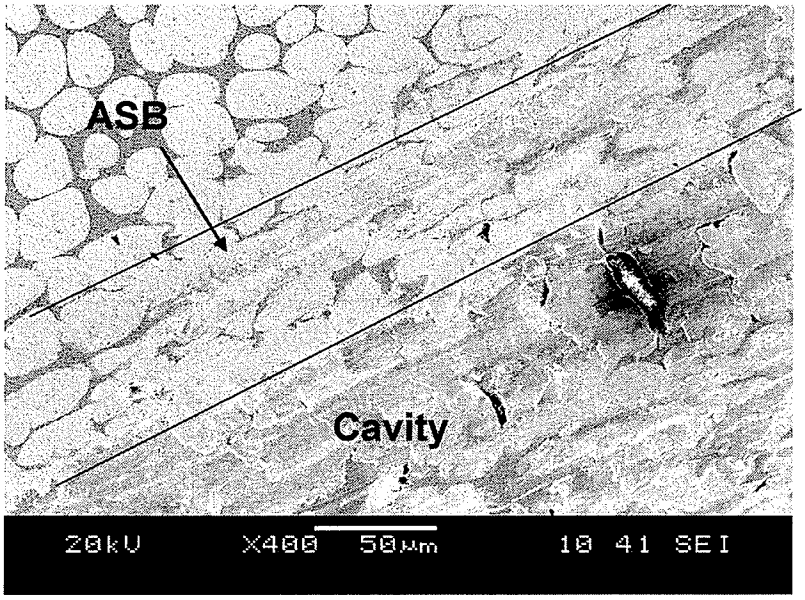

Fig 4.27: SEM micrograph showing deformed band in Tungsten A 90S alloy after high velocity impact momentum of 56.9 kgm/s

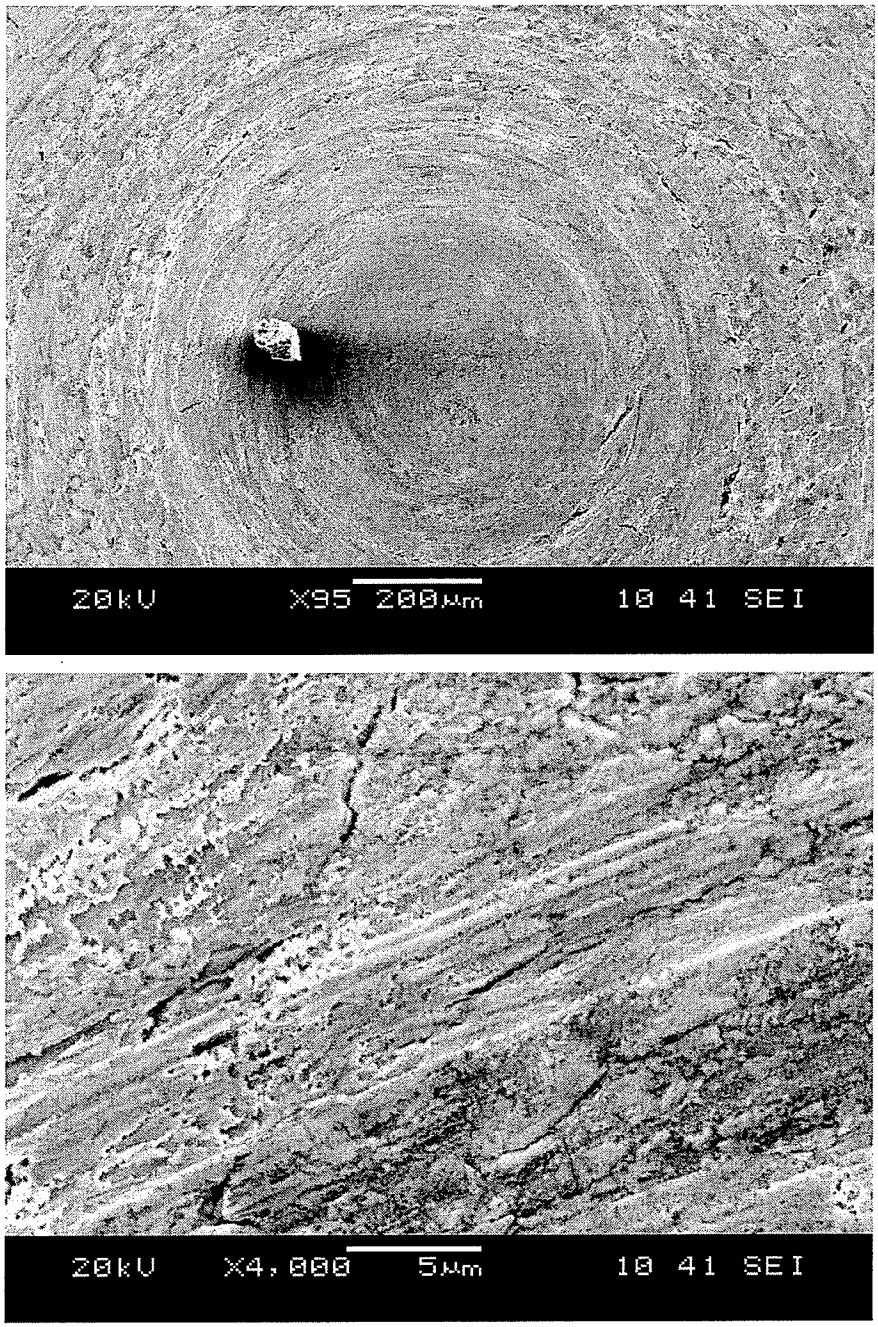

Fig 4.28: SEM micrographs of fracture conical shape fracture surface of Tungsten A90S alloy

Table 4.4: Hardness Measurements (VH) of Tungsten samples

Tungsten Samples	**Average outside of the deformed bands (VH)**	**Average inside of the deformed bands (VH)**
Tu. 1	642	No Shear Bands (NSB)
Tu. 2	653.5	NSB
Tu. 3	645.5	NSB
Tu. 4	657.5	NSB
Tu. 5	698	806.6
Tu. 6	712	775

4.5 Discussion

Table 4.1 shows the experimental data for the high velocity impact of the test specimens for the steel, aluminum, and tungsten samples.

Fig 4.1 shows the flow stress in steel samples increases initially with strain, reaching a maximum value and decreases with subsequent increase in strain. Thermal softening dominates the later stage of deformation leading to stress drop at high strain values.

Similar behavior is observed in tungsten samples while typical stress-strain curves obtained are presented in Fig 4.2. In RHA steel and tungsten A90S alloys, the maximum flow stress before stress drop is influenced by the impact momentum of the projectile. The ultimate stress increases initially with increasing impact momentum reaching a maximum at a critical value of the impact momentum, and decreases with further increase in impact momentum. The initial increase in maximum flow stress with increase in impact momentum is due to the strain hardening effect of plastic deformation. Beyond the critical value, thermal softening and occurrence of adiabatic shear bands, as a result of increased adiabatic heating, plays a more dominant role over strain hardening leading to the observed decrease in the maximum flow stress.

Typical stress strain curves obtained from high strain-rate testing of the Aluminum 5083 are presented in Fig 4.3. In aluminum alloys, the maximum flow stress does not vary with increasing the impact momentum because the thermal softening effects of adiabatic heating dominates deformation to the extent that the increase in strain hardening effects of increasing impact momentum is quickly nullified by thermal softening and adiabatic shear banding.

Comparing the dynamic stress strain behavior of RHA Steel, Tungsten A 90S and Aluminum 5083 at impact momentum of 45.5 kg.m/s shows that the flow stress of RHA Steel and Tungsten A90S are comparable at this strain rate and they are much higher than that of the Aluminum alloys (see Fig 4.7).This shows that steel and tungsten can withstand higher stress at high strain rates than aluminum before adiabatic shear failure.

Fig 4.4 and Fig 4.5 show the comparative evaluation of the engineering strain and strain rates produced in the investigated alloys as a function of the impact momentum of the striker bar. The higher the firing pressure, the higher the impact momentum. The higher the impact momentum, the higher the strain rates generated in the specimens.

It is observed that aluminum alloy has the lowest resistance to plastic deformation while tungsten alloys have the highest resistance to plastic deformation. The slope of the engineering strain against impact momentum is 0.202, 0.014, and 0.012 for Aluminum 5083, RHA Steel, and Tungsten A 90S respectively, therefore aluminum alloy is more ductile compare to tungsten and steel.

The RHA steel exhibits a plate-like microstructure which is typical of a martensitic structure. Optical microscopic examination of the samples after impact test shows that steel samples impacted at a momentum below 44.5 kg.m/s do not show any shear bands due to the low impact momentum and consequently low strain rate. (Figs 4.8 and 4.9). As the impact momentum exceeds 44.5 kg.m/s, the deformed bands appears in the steel sample (Fig 4.10). This shows that adiabatic heating leading to ASBs plays a major role in the deformation process and fracture behavior of the steel samples at impact momentum above 44.5 kg.m/s. As the impact momentum continues to increase, more transformed bands or the white etching bands appear in the steel samples (Figs 4.11, 4.12

and 4.13). The width of shear bands also increases with increasing impact momentum. This is because the more the impact momentum the more the energy that applies to the material and the adiabatically heated zone gets larger and that results in thicker shear bands (Table 4.1). It is clear that before the failure occurs, the shear bands spread out in the material and that causes the initiation of the cracks and failure of the material at high impact momentum of 59.3 kg.m/s (Fig. 4.15). The hardness of the shear bands in steel samples is higher that the bulk material (Table 4.1) and also the hardness increases with increasing the impact momentum (Fig 4.20)

Under high strain rate testing, aluminum alloys show strain localization and adiabatic shear bands. It can be seen from Figs 4.21- 4.23 that formation of ASBs in aluminum alloys are in the form of deformed bands rather that transformed bands. Shear bands formed in aluminum alloys have lower tendencies to cracking than the shear bands formed in steel and tungsten because as the impact momentum continuously increases, the aluminum samples keeps deforming rather than breaking which was observed in steel and aluminum samples. The hardness of the shear bands in the Aluminum alloy is also higher that the bulk material as it is observes in the steel samples (Table 4.3).

Results of the investigation on the tungsten alloy, as seen in Fig 4.25, show that as the impact momentum exceeds 50 kg.m/s, parts of fragments flaked off from the specimen leaving behind conical shape cavities on the surface of the specimen. The conical shape of the cavity is similar to that of the white etching bands formed in steel specimens after high velocity impact test. Such detachment of fragments was not observed in the aluminum alloy or RHA Steel. The extreme strain localization along the shear bands may causes this immediate cracking and fracture along the shear bands in the

tungsten alloy. According to Owolabi et al [33], the low strain-rate sensitivity in tungsten alloy causes the formation of adiabatic shear bands.

Scanning Electron Microscopy (SEM) examination of tungsten alloy proves the occurrence of shear bands formation at the point where the fragments are detached from the test specimen (Fig 4.27). The deformed bands in tungsten alloy consist of distorted and elongated grains. SEM investigations also show the ring shape of the surface cavity.

The hardness of the shear bands in tungsten alloys is higher than that of the bulk material as observed in RHA steel and aluminum alloy (Table 4.4).

Results of the investigation show that the stress collapse time and the critical strain required for the stress collapse leading to mechanical instability, loss of load carrying capacity and ultimately to strain localization are significantly influenced by strain rates and microstructure. In the present study the influence of strain rate on shear localization agrees with Chichili and Ramesh [27] investigation which showed that the shear localization in tungsten alloy is highly dependent on strain rate. The higher the strain rate, the faster the stress collapsed time and the earlier the onset and occurrence of adiabatic shear bands. Plastic deformation and failure of the tested materials at high strain rate are dominated by occurrence of adiabatic shear bands.

By looking at the results of RHA Steel and tungsten A90S after impact it is clear that ASBs formed in these two materials are the cause of crack initiation and propagation and eventually failure of material.

Most failures at high strain rate are the result of strain localization and formation of adiabatic shear bands, because adiabatic shear bands are microstructural imperfection that can generate early failure in the material at high strain rates. Marchand and Duffy [4]

have also proved that shear bands are initiated at a point in the test section and propagate rapidly as deformation proceeds.

As previously mentioned, there are two kinds of shear bands identified in the literature: deformed and transformed bands. Deformed bands appear as severely distorted region showing extensive shear deformation. This type of shear bands was observed in the aluminum and tungsten alloy and in RHA steel at impact momentum below 48 kg.m/s. The other type of shear bands are called transformed band or the white etching bands which is observed in RHA Steel at impact momentum above 48 kg.m/s and were not observed in the aluminum and tungsten alloy. The white color of the bands is because of the phase transformation that occurs in the steel samples during the testing as a result of the increase in the temperature inside the shear band. It has been suggested that the white colure of the bands is the product of austenite to untempered martensite during adiabatic shearing [41]. Several TEM studies on white ASB in steel have shown that the shear bands consist of very fine cells less than 100 nm in size [20, 42]. Meyers and Wittman [20] reported that the white etching band in steel samples consist of fine Fe_5C_2 Carbides and very fine martensite laths and suggested that white etching forms because the dissolution of carbide changes the etching characteristics of the shear band.

Armstrong and Zerilli [26] suggested that softening and the local rise in temperature in the material can happen when a dislocation pile up cut through a grain boundary and it creates a site for shear band initiation and shear propagation while it is high enough to cause the phase change in steel and lead to changes in strength and other mechanical properties.

Cho *et al.* [24] suggested that the mechanism for formation of transformed band in pearlitic steel consists of elongation and fragmentation of the grains into very fine sub-grains along the band of intense strain localization. Zurek [15] also reported extremely fine nanosized grains inside transformed bands in steel and suggested that the resolution limit of optical microscope in resolving the nanostructure of the transformed band accounts for white color of transformed bands.

Li *et al.* [29] also reported that at high strain rate the failure of titanium alloy Ti-17 is more sensitive to strain rate than to the applied stress level. Odeshi *et al.* [43] suggested that the type of shear bands formed in steel samples depends on the extent of fragmentation which depends on the velocity of the impact during testing. The velocity of the impact determines the impact momentum.

In the present study, the steel samples showed no shear bands below impact momentum of 48 kg.m/s. This is because the impact velocity is not high enough to cause the initiation of the shear bands. According to Bonnet-Lebouvier *et al.* [44] there is a threshold impact momentum, below which no shear bands propagation is obtainable. That minimum impact momentum required for the shear bands to occur for our steel specimens is 48 kg/s. Between the impacts momentum of 48 kg.m/s and 56 kg.m/s the only type of shear bands that forms in the investigated steel samples are the deformed bands. Furthermore above the impact momentum of 56 kg.m/s the transform bands or the white etching bands occur. Therefore, we can conclude that the strain rate produced by the applied impact momentum below 48 kg.m/s in RHA steel des not meet the required minimum strain rate to cause the initiation of the shear bands. At impact momentum of above 48 kg.m/s and below 56 kg.m/s, the corresponding strain rate is not sufficiently

high to cause occurrence of transformed band, but sufficient enough to trigger formation of deformed band consisting of distorted grains. At impact momentum above 56 kg.m/s intense strain localization leading to formation of transformed bands occurs and at impact momentum in excess of 58 kg.m/s, the transformed shear bands crack extensively leading to specimens' fracture. Some cracks are observed in steel specimen impacted at 56.3 kg.m/s. With increasing impact momentum, these cracks will propagate and cause failure.

A correlation is observed between the results of dynamic mechanical loading and microstructure of the samples. As the impact momentum of RHA Steel and tungsten samples increases, the maximum flow stress increases until the applied impact momentum is high enough to trigger the formation of ASBs and then the maximum flow stress begins to decrease with further increase in impact momentum. At this point, the flow stress is dominated by thermal softening, extreme strain localization and occurrence of adiabatic shear bands.

Low strain-rate sensitivity in the tungsten alloy causes the formation of ASBs [35]. In tungsten at the low impact momentum (below 52 kg.m/s), no shear bands was observed. Therefore, the minimum impact momentum for tungsten alloy to show shear bands is 52 kg.m/s. Above this impact momentum, pieces of tungsten flaked off from the specimen. This detachment of fragments is because of the formation of ASBs which are extremely brittle. SEM examination of Tungsten alloy proves the occurrence of shear bands formation at the point where the fragments are detached from the test specimen. The shear bands, once initiated in tungsten cracked leading to fracture of the specimen. The strain rate produced by the applied impact momentum above 52 Kg.m/s is high enough to

initiate and propagate the shear band and cause the immediate cracking and fracture in the tungsten alloy.

For aluminum alloy, plastic deformation is dominated by adiabatic heating and occurrence of ASBs and there was no significant change in maximum flow stress as the impact momentum was increased within the range of the applied impact momentum. In aluminum, ASBs could be initiated with impact momentum as low as 29 kg.m/s. The type of ASBs observed in the aluminum alloy is the deformed type.

As previously mentioned, the hardness of the shear bands in RHA Steel, Tungsten, and aluminum alloys is higher than the hardness outside shear bands. Grain boundaries act as barriers to motion of dislocation during plastic deformation. Increased grain boundary as the results of grain modification due to shear bands will therefore lead to higher resistance to plastic deformation and therefore to increased hardness inside shear bands. Shear bands have finer grain size compared to the region outside the shear bands. The higher hardness of shear bands could be the results of finer grain size and the extreme localization of shear strain in the shear band region [43]. Rogers and Shasty [19] also observed that the hardness of white etching bands in steel was dependent on carbon content.

Microstructural evolution of white etching bands in martensitic steel after high strain rate deformation by Wingrove [45] showed shear bands consist of high density dislocation and extremely fine cell boundaries.

In this investigation, it was observed that the hardness measured inside the shear bands is higher than that measured outside shear bands in the steel, aluminum, and tungsten specimens because there are significant increases in dislocations within the

bands in these samples (Tables 4.2 - 4.4). This investigation also shows that the hardness of the white etching bands in steel samples increases with increasing impact momentum. This may be the result of increased intensity of grain fragmentation and dislocation generation inside the shear bands during impact at higher impact momentum. (Fig 4.20)

5 Chapter 5: Conclusions

The main objective of this research was to investigate the formation of ASBs in selected armor materials that were tested at high strain rate using Direct Impact Hopkinson Pressure Bar at strain rates in excess of 10^3 S^{-1}. Dynamic stress-strain responses for each group of samples were generated to provide information on mechanical properties of these materials.

Microstructural evolution in the material during high strain-rate deformation is also investigated. The following conclusions can be made from the results of the experimental investigations:

- Occurrence of shear bands has a major influence on dynamic stress-strain curves for the materials and causes failure at high strain rates.
- Occurrence of ASBs depends on the type of the material that is been investigated.
- The ASBs formed during the impact loading of the steel samples are either deformed bands or white etching bands depending on the impact momentum, but in aluminum and tungsten, there are only deformed bands present when observed under the optical microscope.
- The width of shear bands in steel samples increases with increasing impact momentum.
- The micro hardness measurements showed that the hardness values inside the adiabatic shear band in all specimens are much higher than in the bulk material.

This may be due to the high dislocation density and finer structure inside the shear bands.

- Hardness of the shear bands in impacted RHA steel samples increases with increasing impact momentum due to increase intensity of strain localization, grains fragmentation and dislocation generation inside the shear bands.
- The ASBs are a preferred path for crack initiation and propagation leading to fracture of the specimens.
- Shear bands formed in aluminum alloy is deformed. They get darker with increasing the impact momentum.
- Shear bands formed in aluminum alloy have less cracking tendencies than the shear bands formed in steel and tungsten alloy.
- As the impact momentum increases for RHA Steel and tungsten alloy, the maximum flow stress increases until it reaches the impact momentum that causes the formation of ASBs and then starts to decrease with further increase in impact momentum. At this impact momentum, the flow stress is dominated by thermal softening, extreme strain localization and occurrence of adiabatic shear bands.
- As the impact momentum increase in aluminum, there is no significant changes in maximum flow stress, and the plastic deformation is dominated by adiabatic heating and occurrence of shear bands.
- The ASBs formed in tungsten are very brittle and cause flaking of the material.
- Aluminum 5083 alloy exhibits the lowest strength compared with RHA steel and tungsten A90S alloy and is more ductile. It also shows the least tendency to cracking than tungsten and steel.

REFERENCES

[1] Al-Ameeri, S, "The effect of heat treatment on the adiabatic shear bands in AISI 4340 steel at high strain rate", MSc thesis 2005, University of Manitoba

[2] Ductile and Brittle material and their properties,
http:// invsee.asu.edu/srinivas/stress-strain/ssgraph.jpg

[3] Callister, W .D. Jr., Material, science and Engineering –An Introduction, 5th ed., John Wiley & Sons, Inc., New York, 2000

[4] Marchand, A., and Duffy, J., "An experimental study of the formation process of adiabatic shear bands in a structural steel", journal of Mechanics and Physics of Solids, 36 (1988) 251–283

[5] Anderson, D.D., and Rosakis, A.J., "Comparison of three real time techniques for the measurement of dynamic fracture initiation toughness in metal", Engineering Fracture Mechanics, 72(2005), 535-555

[6] Schoenfeld, S.E., and Wright, T.W., "A failure criterion based on material instability", Int. J. Solids Structure, 40(2003), 3021–3037.

[7] Odeshi, A.G., Al-ameeri, S., Bassim, M.N., "Effect of high strain rate on plastic deformation of a low alloy steel subjected to ballistic impact", Materials Processing Technology,162 (2005), 385-391.

[8] Turley Doyle, E.D., and Ramaligam, S., "Calculation of shear strains in chip formation in titanium", Material Science and Engineering (1982) 45-55

[9] Dao, K.C., and Schockey, D.A., "A method for measuring shear band temperature", Journal of Applied. Phys. 50 (1979), 8244

[10] Raftenberg, M.N., and Krause, C.D., "Metallographic observations of armor steel specimens from plates perforated by shaped charge jets", Int. J. Impact Eng. 23(1999), 757–770.

[11] Erlich, D.C., Seaman, L., Schockey, D.A., and Curran, D.R., "Development and application of a computational shear band model", BRL-CR-00416.

[12] Bassim M.N., "Study of the formation of adiabatic shear bands in steel", Proceedings of the 11th International Conference on Experimental Mechanics, 119(1998) 234-236

[13] Odeshi, A.G., Bassim, M.N., and Al-Ameeri, S., "Effect of heat treatment on adiabatic shear bands in high-strength low alloy steel", Material Science and Engineering, A 419 (2006), 69-75.

[14] Odeshi, A.G., Al-ameeri, S., Mirfakhraei, S., Yazdani, F., and Bassim, M.N., "Deformation and failure mechanism in AISI 4340 steel under ballistic impact", Theoretical and Applied Fracture Mechanics, 45(2006), 18-24

[15] Zurek, A.k., "The study of adiabatic shear bands instability in pearlitic 4340 steel using a dynamic punch test", Metallurgical and Materials Transactions, 25A (1994), 2483-2489

[16] Hartly, A., Duffy, J., and Hawely, R.H., Journal of Mechanics and Physics of solids 35(1987), 283-301

[17] Feng, H., and Bassim, M.N., Finite element modeling of the formation of adiabatic shear bands in AISI 4340 steel, Materials science and Engineering a 266(1999) 255-260

[18] Zhange, B., Shen, W., Liu Y. , Zhange, R., "Some factors influencing adiabatic shear bands in impact wear", 214(1998), 259-263

[19] Rogers, H.C., Shastry, C.V., "Materials factors in adiabatic sharing in steel", plenum press, New York, 1986, pp. 285-298.

[20] Meyers, M.A, Wittman C.L., "The effect of metallurgical parameter on shear band formation in low-carbon (~0.20 Pct) steel", Metal Trans 21A (1990) 3153-3164

[21] Chen, Z.H., Chan Lee, T.C., and Tang, C.Y., "An investigation on the formation and propagation of shear band in fine-blanking process", Journal of Material Processing Technology, 138(2003), 610–614

[22] Glenn, R.C., and Leslie, W.C., "The nature of "white Streaks" in impacted armor steel plate", Metallurgical Transactions, 2(1971), 2945–2947

[23] Derep, J.L., "Microstructure transformation induced by adiabatic sharing in armored steel", Acta Metal, 35(1987), 1245-12498

[24] Cho, K-M., Lee, S., Nutt, S.R., Duffy, J., "Adiabatic shear bands formations during dynamic torsional deformation of an HY-100 steel", Acta Metal. 41 (1993) 923-932

[25] Meyers, M.A., Xue, Xu Q., Perez-Prado, M. T., and Mcnelley, T.R., "Microstructural evolution in adiabatic shear band localization in stainless steel", Acta Material 51(2003) 1307-1325

[26] Armstrong R.W., and Zerilli, F.J., "Dislocation mechanics aspects of plastic instability and shear bending", Mechanics of Materials, 17 (1994) 319-327

[27] Chichili, D.R., Ramesh, K.T., Hemker, K., "Adiabatic shear localization in α-titanium": experiments, modeling and microstructural evolution, Journal of Mechanics and Physics of Solids, 52(2004) 1889-1909

[28] Right T.W., and Walter, J.W., "On stress collapse in adiabatic shear bands", Journal of Mechanics and Physics of Solids, 35(1987) 701-720

[29] Qiang, Li, Yongbo, Xu, and Bassim M.N., "Dynamic mechanical properties in relation to adiabatic shear band formation in titanium alloy –Ti17", Material Science and Engineering,358 (2003)P128-133

[30] Anand, L., and Kalidindi, S.R., Mech of Mat, 17(1994)223

[31] Xue, Q., Meyers, M.A., Nesterenko, V.F., "Self organization of shear bands in titanium and Ti-6Al-4V alloy", Acta Material 50(2002) 575-596

[32] El-Magd E., and Brodmann, M., "Ductility of aluminum alloy AA7075 at high strain rates", J.Phys .IV France 10(2000)

[33] Owalabi, G.M., Odeshi, A.G., Singh, M.N.K., and Bassim, M.N., "Dynamic shear band formation in Aluminum 6061-T6 and aluminum 6061-T6/ Al_2O_3 composites", Material Science and Engineering, A 457(2007) 114-119

[34] Li, J.R., Yu, J.L., Wei, Z.G., "Influence of specimen geometry on adiabatic shear instability of Tungsten heavy alloys", International journal of Impact Engineering 28(2003), 303-314

[35] Dong-kuk Kim, Sunghak Lee, and Woon Hyung Baek, "Microstructural study of adiabatic shear bands formed by high-speed impact in a tungsten heavy alloy penetrator", Material science and engineering, A 249(1998), 197-205

[36] Boss, A., Couque, H., and Lankford, J., "Shear localization in tungsten heavy alloys", Inter. J. Powder Metallurgy.

[37] Meyers, M.A., Dynamic failure: Mechanical and Microstructural aspects, Journal de Physique III 6 (1994) C8-597-621

[38] Erlich, D.C., Curran, D.R., and Seaman, L., "Further development of a shear band model". Final Report to the Army Materials and Mechanics Research Center, Report AMMRC TR 80-3, SRI Int., Menlo Park, CA, 1980, p. 51.

[39] Rogers, H.C: Ann Rev .Material .Sic, 1979, vol9, pp.238-311

[40] Duffy, J., and Chi, Y. C., "On the measurement of local strain and temperature during the formation of adiabatic shear bands", Material Science and engineering A, 257 (1992) 195-210

[41] Glenn, R. C., and Leslie, W.C.,: Metallurgical Transactions, vol. 2(1971) 2945-2947

[42] Barry, J., Bryne, G., "TEM study on the surface white layer in two turned hardened steel", Materials science and Engineering, A 325(2002) 356-364

[43] Bassim M.N., and Odeshi, A.G., "Microstructural evolution in dual phase steel at high strain rates", Materials Science Engineering A(2007), doi:10.1016/j.msea.2007.11.021

[44] Bonnet –Lebouvier, A.S., Molinari, A., Lipinski, P., "Analysis of dynamic propagation of adiabatic shear bands", International journals of solids and structures, 39 (2002) 4249-4269

[45] Wingrove, A.L., journal of Australian Institute of Metals 16 (1971) 67-70